Cell adaptive response to extracellular matrix density is controlled by ICAP-1-dependent beta1-integrin affinity.

Angélique Millon-Frémillon, Daniel Bouvard, Alexei Grichine, Sandra Manet-Dupé, Marc R. Block, Corinne Albiges-Rizo

Cell adaptive response to extracellular matrix density is controlled by ICAP-1 dependent β_1 integrin affinity

Angélique Millon-Frémillon[1,2,3], Daniel Bouvard[1,2,3], Alexei Grichine[2,4], Sandra Manet-Dupé[1,2,3], Marc R. Block[1,2,3], Corinne Albiges-Rizo[1,2,3]

[1]: INSERM U823 Institut Albert Bonniot, Equipe DySAD, Site Santé, BP 170, 38042 Grenoble cedex9, France.
[2]: Université Joseph Fourier
[3]: CNRS
[4]: INSERM U823 Institut Albert Bonniot, Cell imaging platform.

Correspondence to Corinne Albiges-Rizo: corinne.albiges-rizo@ujf-grenoble.fr
Tel: 33 476 54 95 50; Fax: 33 476 54 94 25

Condensed title: integrin affinity and focal adhesion dynamics

Keywords: ICAP-1, β_1 integrin affinity, focal adhesion dynamics, extracellular matrix sensing.

Character count including all sections except the materials and methods and references: 36438

Revised manuscript sent the 15th of November 2007.
Manuscript number: JCB200707042

Abstract

Cell migration is an integrated process requiring the continuous, coordinated assembly and disassembly of adhesion structures. How cells orchestrate adhesion turnover is only partially understood. We provide evidence for a novel mechanistic insight into focal adhesion dynamics by demonstrating that ICAP-1 (Integrin Cytoplasmic domain Associated Protein 1) slows down focal adhesion assembly. Live cell imaging, performed in both *Icap-1* deficient mouse embryonic fibroblasts and cells expressing active β_1 integrin, shows that the integrin high affinity state favoured by talin is antagonistically controlled by ICAP-1. This affinity switch results in the modulation in the speed of focal adhesion assembly and, consequently, of cell spreading and migration. Unexpectedly, the ICAP-1 dependent decrease in integrin affinity allows cell sensing of matrix surface density suggesting that integrin conformational changes play a key role in mechanotransduction. Our results clarify the role of ICAP-1 in cell adhesion and highlight the central role it plays in the cell's integrated response to the extracellular micro-environment.

Introduction

Adhesion to ECM is primarily mediated by integrins, a family of heterodimeric receptors (Hynes, 2002) that cluster into adhesion sites. Focal adhesions (FA) have been shown to form a scaffold that first sense then transform extracellular cues into cellular responses and in turn transmit the contractile intracellular tensions to the ECM (Bershadsky et al., 2003; Chen et al., 2004; Ingber, 2003). Because of their involvement in cell motility and matrix remodeling, adhesion sites are necessarily dynamic structures able to assemble and disassemble. FA assembly takes place at the leading edge of membrane protrusions, whereas disassembly occurs both at the cell rear and at the base of protrusions. The molecular mechanisms controlling FA turnover have been partly characterized. They require Rho family GTPases, integrin engagement, coordinated interaction between integrins and structural/signaling molecules, as well as actin-binding proteins, actin microfilaments and microtubules (Ezratty et al., 2005; Raftopoulou and Hall, 2004; Webb et al., 2004). Talin, a direct cytoplasmic β integrin binding protein, is involved in adhesion site formation, reinforcement and stabilization (Albiges-Rizo et al., 1995; Giannone et al., 2003; Jiang et al., 2003; Priddle et al., 1998), as well as in integrin activation and local PIP2 generation (Calderwood et al., 2002; Martel et al., 2001; Tadokoro et al., 2003). Integrin clustering requires the formation of complexes composed of activated integrins, immobilized ligands, talin and PIP_2 (Cluzel et al., 2005). Additionally, the calpain family regulates cell motility, partly by down regulating integrin-mediated adhesion complexes (Bhatt et al., 2002) and through talin cleavage a rate-limiting step during adhesion turnover and critical for FA disassembly (Franco et al., 2004). The current understanding is that integrin containing adhesion sites function as signal transduction centers. Consequently tight regulation of integrin affinity is crucial for adhesion signaling (Bennett, 2005). Integrins adopt high- and low-affinity conformations, and ligand-integrin binding is often preceded by intracellular changes, resulting in increased affinity (Ginsberg et al., 2005). Crystal structure analysis suggests a bent, hook-like conformation for the extracellular domain in the inactive state and an extended conformation in the active state (Liddington and Ginsberg, 2002; Takagi and Springer, 2002). Talin binding disrupts a salt bridge between the α and β subunits leading to integrin activation (Luo et al., 2004; Vinogradova et al., 2004). Evidence suggests that the binding of a complex including talin, RIAM, Rap1 and VASP to the integrin cytoplasmic tail is a common final step in integrin activation (Han et al., 2006).

Among integrin partners, ICAP-1 encompassing a PTB domain interacts specifically with the cytoplasmic tail of β_1 integrin at the membrane distal NPXY motif. The increase of β_1 integrin dependent cell motility on fibronectin (FN) upon ICAP-1 over-expression (Chang et al., 2002; Chang et al., 1997; Zhang and Hemler, 1999) and cell rounding up after overexpression of a phosphomimetic mutant of ICAP-1 at the CaMKII site (Bouvard and Block, 1998) suggest that ICAP-1 regulates β_1 integrin function. Moreover, talin and ICAP-1 compete in vitro for integrin binding and high ICAP-1 concentrations disrupt FA (Bouvard et al., 2003). ICAP-1 and β_1 integrin are colocalized at the leading edges of cells during the early stages of spreading (Fournier et al., 2002). This facet, obviously regulatory and transitory, of ICAP-1 in FA dynamics prompted us to determine in more detail the role played by ICAP-1 in adhesion site dynamics.

Here we show that *Icap-1* deficient MEF display defects in cellular spreading and migration correlating with redistribution of FA, a modification in FA dynamics, and an increase in integrin affinity. These defects could be mimicked by increasing either integrin affinity or the surface density of the underlying matrix. By modulating integrin affinity, ICAP-1 allows the cell to adapt its adhesion strength and rate of migration to changes in the matrix surface density. These data point not only to the existence of specific molecules involved in FA assembly or disassembly signaling pathways but also to the control of FA assembly and matrix sensing through fine tuning of integrin affinity.

Results

ICAP-1 loss alters the distribution and morphometry of FA

To figure out the role of ICAP-1 in FA dynamics, we compared the adhesive behavior of MEF isolated from WT and *Icap-1* deficient mice embryos as well as in WT, *Icap-1* null and *Icap-1* rescued osteoblasts. Immunostaining revealed paxillin and β_1 integrin containing FA to be distributed throughout the ventral cell surface in *Icap-1* null MEF while WT cells exhibited mostly peripheral FA (Fig. 1A). In contrast the distribution of the β_3 integrin (known not to interact with ICAP-1) containing FA was not modified in *Icap-1* null cells (Fig. S1A). FA distribution defects were ICAP-1 dependent and not cell specific since centrally located FA in *Icap-1* null osteoblasts were redistributed peripherally after *Icap-1* rescue (Fig 1B). This altered FA distribution was also associated with a modification of their morphometry. β_1 integrin containing FA on FN were significantly larger in *Icap-1* null fibroblasts, whereas the size of β_3 integrin containing FA remained identical for both cell types (Fig.1C). β_1 integrin clustering within FA, estimated by the mean fluorescence intensity, was increased by about 2 fold in *Icap-1* null cells compared to WT cells (Fig.1C). Then we analyzed the putative role of ICAP-1 in the regulation of FA composition (Fig. 1D). Talin, vinculin, and paxillin as well as surface β_1 and β_3 integrins were expressed at similar levels in both cell types (Fig. S1B and C). Constant adaptor protein/integrin ratios in both cell types indicates that ICAP-1 did not interfere with FA constitution and revealed that β_1 integrins highly clustered within FA in null cells are fully competent to bind their intracellular partners (Fig. 1D). Thus the increased size of FA in *Icap-1* null MEF could be attributed to increased β_1 integrin clustering and not to an indirect change in adhesion proteins expression or to a modification in cell surface expression of β_3 and β_1 integrins.

Icap-1 null cells exhibits a shift in the optimum ECM surface density required for cell migration and spreading

As the modification in the FA pattern and morphometry reflects cell adhesion and migratory defects, we monitored the migration rate of MEF spread on increasing concentrations of β1 integrins engaging matrices, FN and type I collagen (CL). The typical bell-shaped curve observed for WT cells was shifted toward the lower densities of ECM substrates for *Icap-1* deficient cells. Indeed, the optimal matrix concentration required for maximum migration of *Icap-1* deficient cells was reduced 10 fold and 20 fold for FN and CL coatings respectively

(Fig. 2A). A very similar result was obtained with FN using time-lapse videomicroscopy (Fig. 2B).

Since migratory properties were modified in *Icap-1* null MEF, we investigated the consequences of ICAP-1 loss on cell spreading. The densities required to reach similar spreading levels on both matrices were much lower with *Icap-1* null cells than with WT cells. Indeed, with FN: 50% spreading was achieved at 0.5 µg/ml coating concentration for *Icap-1* null cells, versus 1 µg/ml for WT cells (Fig 2C). Similar results were obtained with CL: 50% spreading occurred at a coating concentration of 5 µg/ml for *Icap-1* null cells compared to 25 µg/ml for WT cells (Fig. 2C). *Icap-1* null cells appeared to exhibit a stronger interaction with FN and CL, and consequently spread at lower densities of these ECM substrates. In both migration and spreading assays, the differences between WT and mutant cells were more pronounced using CL. This probably reflects the more restricted use of β_1 integrins on CL. On the other hand, expression of ICAP-1 in *Icap-1* null MEF restore cell spreading and migration similarly to that was observed for WT MEF (Fig. S2A and S2B), proving that the altered migration was indeed due to the loss of endogenous ICAP-1. A similar effect was also observed with osteoblasts: at the FN coating concentration of 0.3 µg/ml, the totality of *Icap-1* null osteoblasts were fully spread while only 50% of WT and rescued osteoblasts were spread under identical experimental conditions, demonstrating that this defect was still ICAP-1 dependent but not cell specific (Fig 2D). In good agreement with the specificity of ICAP-1 for β1 integrin, migration and adhesion behaviours of WT and *Icap-1* null MEF on vitronectin (VN) were not significantly different. This demonstrates that ICAP-1 loss did not alter β_3 integrin mediated adhesion (Fig. S3A and S3B).

ICAP-1 slows down the talin recruitment into FA

The fact that *Icap-1* null cells migrated and spread at lower matrix densities might reflect defects in adhesion dynamics. If ICAP-1 was involved in FA dynamics, differences are expected in the exchange or recruitment rate of some FA components between *Icap-1* null cells and WT cells. To address this point, measurements of fluorescence recovery after photobleaching experiments were made using EGFP fused vinculin or talin (Fig. 3). Single FA in the lamella was photobleached and their fluorescence recovery recorded. Recovery times (τ) were calculated for both fusion proteins. Our results revealed that EGFP-vinculin recruitment was 4 times faster than EGFP-talin in WT MEF cells spread on FN (Fig. 3A). However, no difference between WT and *Icap-1* deficient MEF was observed in the

incorporation speed of EGFP-vinculin into FA demonstrating that vinculin recruitment is ICAP-1 independent. Conversely, the recovery half-time associated with EGFP-talin was significantly lower in *Icap-1* deficient MEF, suggesting a faster recruitment of EGFP-talin in cells lacking ICAP-1. This conclusion is in line with the proposed competitive binding of ICAP-1 and talin for the β_1 integrin cytoplasmic domain (Bouvard et al., 2003). FRAP experiments were also performed in cells spread on β_3 integrin preferential substrate, such as VN in order to compare talin and vinculin recruitment in case of *Icap-1* deficiency (Fig. 3B). As expected no significant change in talin recruitment was observed in both cells spread on VN. Our results demonstrate that the function of ICAP-1 is dependent on adhesion on specific substrate.

ICAP-1 slows down FA assembly

Two key steps in cell migration are FA assembly and disassembly (Webb et al., 2004). To identify whether ICAP-1 was involved in FA turnover, WT and *Icap-1* null MEF cells expressing EGFP-VASP, EGFP-paxillin or EGFP-vinculin were monitored using time-lapse video-microscopy over a 6 hours period. Again we noticed that EGFP-VASP (Fig. 4A), EGFP-paxillin or EGFP-vinculin (not shown) expressed in *Icap-1* null cells were mostly localized in central FA. Cells were plated on a low concentration of FN (1 μg/ml) in order to favor cell migration. Turnover of FA located at the cell leading edge were arbitrary decomposed into four parameters: namely, assembly (from the first appearance until the maximal pixel intensity level is reached), steady state duration (no change of the maximal pixel intensity), disassembly rates (from the maximum pixel intensity is reached until focal adhesion is not resolvable), and total lifetime (from the first appearance of a resolvable focal adhesion until its disappearance). In *Icap-1* null cells, the increase in EGFP-tagged proteins intensity during FA assembly was significantly faster (Fig. 4B and 4F) and the duration of the steady state was slightly shorter (Fig. 4D) than for WT cells. In contrast, FA disassembly rates (Fig. 4C and 4F) were identical for both cell types. These measurements showed that faster FA assembly associated with a minor reduction of the steady state upon ICAP-1 loss result in a shorter FA lifetime (Fig. 4E and 4F). It is worth noting that this change in dynamics was not observed with *Icap-1*$^{-/-}$ cells spread on VN, thus underlining the action of ICAP-1 on β_1 integrins (Fig. S3C). Altogether these data suggest that ICAP-1 down regulates cell migration and spreading by slowing down FA assembly involving β_1 integrins.

ICAP-1 is not required for FA disassembly

Previous work has highlighted an important role for microtubule networks in FA turn-over (Ezratty et al., 2005; Kaverina et al., 1999). This is based on the finding that microtubule depolymerization upon nocodazole treatment increases FA assembly whereas microtubule regrowth after nocodazole washout induces a rapid and reversible disassembly of FA. We took advantage of the synchronized disassembly of FA induced by nocodazole to investigate the involvement of ICAP-1 in the control of this process. After 4 h of nocodazole treatment the microtubule network totally collapsed and WT MEF displayed larger peripheral FA (Fig. 5A and 5B). However, *Icap-1* deficient MEF showed a dramatic increased in the number of central FA whereas the number and size of peripheral FA were not significantly changed (Fig. 5A and 5B). For both cell types, 60 min after nocodazole washout, FA disassembly temporally coincided with *de novo* growth of microtubules towards the cell periphery. FA reappeared 90 min after nocodazole washout, showing that FA disassembly was reversible in both cell types. Quantification of our observations revealed that nocodazole treatment of *Icap-1* null cells induced *de novo* formation of central but not peripheral FA. By contrast, WT MEF behaved differently since nocodazole induced a reinforcement of existing peripheral FA without promoting *de novo* assembly (Fig. 5B). Along with the video-microscopy experiments these results consistently suggested that ICAP-1 loss favored FA assembly but had no influence on disassembly.

Increased integrin affinity in *Icap-1* deficient cells is responsible for the cell adhesion phenotype

As ICAP-1 competes with talin for β_1 cytoplasmic domain binding (Bouvard et al., 2007; Bouvard et al., 2003), the promotion of FA assembly resulting in the modification in migration and spreading of *Icap-1* null fibroblasts could arise from an increase in β_1 integrin affinity. Indeed the activation state of β_1 integrins measured by FACS revealed a higher affinity state in *Icap-1* null cells than in WT cells (Fig. 6A). This result is consistent with our recent work showing an increase in $\alpha_5\beta_1$ integrin affinity in osteoblasts isolated from *Icap-1* null mice (Bouvard et al., 2007) and also suggests that this integrin affinity increase is cell type independent. To correlate the increase in β_1 integrin affinity to the adhesive defect observed in *Icap-1* null cells, integrins were chemically activated in WT cells in order to mimic *Icap-1* null phenotype (Fig 6B-C and S4). Mn^{2+} treatment of both WT and rescued cell types shifted the spreading curve toward lower FN or CL surface densities while it had no

effect on Mn^{2+} treated *Icap-1* null cells since their integrins are already in a high affinity state (Fig. 6B and S4A-B). These results were also confirmed with 9EG7 mAb which is able to both recognize an activated β_1 integrin specific epitope and maintain it in its high affinity conformation (Fig. 6C and S4C). Thus, it was tempting to speculate that β_1 integrin affinity could also control FA assembly. To test this hypothesis we generated the activated β_1 integrin mutant D759A with a disrupted salt bridge between α and β subunits (Hughes et al., 1996; Partridge et al., 2005; Sakai et al., 1998) and expressed it in β_1 integrin deficient GD25 cells. First, we confirmed that GD25/β_1D759A cells displayed a higher affinity for the FNIII7-10 fragment than GD25/β1WT cells (Fig. 7A). At moderate FN surface densities, FA were centrally distributed in GD25/β_1D759A cells while they were located on the periphery in control cells (Fig 7B). Both adhesive and migratory curves displayed a shift toward the lower matrix densities in mutant cells (Fig. 7C). The FN coating concentration giving the highest migration speed was approximately five times lower for GD25/β_1D759A cells. Mn^{2+} treatment of GD25/β1WT integrin cells induced a shift in the spreading curve and mimicked the adhesive behavior of GD25/D759Aβ_1 cells and *Icap-1* null cells. Finally, GD25/β_1D759A cells displayed a faster rate of FA assembly, associated with a shorter lifetime, without any significant modification in the duration of the steady state or the disassembly rate (Fig.7D). Altogether these results suggest that the adhesive defect in *Icap-1* null cells was due to the presence of β_1 integrin in its active state and further implicate β_1 integrin activation in the regulation of FA assembly.

Control of β_1 integrin affinity by ICAP-1 allows ECM density sensing

The reduced amount of adsorbed matrix required to support cell migration or spreading observed for *Icap-1* null cells suggests that the sensing of matrix surface density has been changed. Moreover, the activation of β1 integrin displaces the maximal adhesive response to a significantly lower matrix concentration, suggesting that ICAP-1 is involved in the cell's perception and response to its microenvironment. We hypothesized that increasing substrate density would affect adhesion strength and favour the active state of the integrin into its active state. Indeed, WT MEF on low density matrices showed only peripheral FA (Fig. 8A). At high matrix density, the observed increase in FA number distributed throughout the ventral cell surface was correlated with an increase in activated β_1 integrin recruitment into FA (fig.8B and 8C). However, in *Icap-1* null MEF, FA were mostly distributed all over the ventral face whatever the matrix density used. These results reveal that increasing substrate

density induces β_1 integrin to take up its high affinity state and, furthermore, that ICAP-1 loss renders cells unable to sense the state of the matrix and adapt to variations in ECM density.

To assess whether the reduction in adhesive response of *Icap-1* null cells to matrix density could be attributed to some differential adhesion dynamics, we quantified FA turnover in cells at different FN matrix densities using time-lapse video-microscopy (Fig. 8D). In WT cells, increased matrix density (10-50µg/ml) induced faster FA assembly. A similar effect was observed using *Icap-1* null cells but at lower FN coating densities. This result supported our hypothesis that matrix density affects FA assembly and that *Icap-1* null cells can only poorly adapt their adhesive structures to increase in ECM density because of their already high adhesion strength at low matrix density. However, we noticed a rise in the length steady state phase at higher matrix densities in both WT and null cells suggesting that the control of FA dynamics during the stages following assembly is ICAP-1 independent but matrix density dependent. These results highlight the involvement of ICAP-1 in sensing the state of the matrix state through control of FA assembly, thus enabling the cell to adapt its adhesive response to changes in the properties of the ECM.

Discussion

Herein, we have used both *Icap-1* deficient MEF and active β_1 integrin mutants to show that the regulation of integrin affinity is necessary for the control of FA assembly and consequently also for cell spreading, and cell migration. Our data demonstrate that ICAP-1 slows down FA assembly by decreasing β_1 integrin affinity. We also document a new and unexpected role for ICAP-1 in the regulation of integrin affinity for a proper matrix surface density sensing. Therefore, ICAP-1 belongs to the molecular machinery of the FA able to provide the cell with the ability to respond adaptively to changes in substrate density.

Our present work provides an array of convergent clues in support for a critical role for ICAP-1 in the control of FA turnover. Indeed, the faster assembly rate of FA in the lamella of *Icap-1* null cells accelerates the maturation state of the adhesion and is associated with a slightly shorter steady state resulting in a reduced lifetime. However, as the rate of FA disassembly is not modified by the lack of ICAP-1, this strongly suggests that disassembly is triggered by an ICAP-1 independent signaling pathway. While some proteins such as paxillin and FAK are involved in FA disassembly (Schober et al., 2007; Webb et al., 2004; Zaidel-Bar et al., 2007), to date, ICAP-1 is the only regulatory molecule so far shown to negatively control the assembly phase. The specific interaction of ICAP- 1 with the β_1 integrins (Chang et al., 1997) combined with the change in the adhesion properties of *Icap-1* null cells depending on the integrin engaging substrates, indicate that the observed modification in FA dynamics in these cells probably involves the participation of β_1 integrins.

Modification in the dynamics of β_1 integrin containing FA in *Icap-1* null cells is also revealed by the faster recruitment of EGFP-talin into FA observed by FRAP studies. This observation in living cells fits with *in vitro* talin-ICAP-1 competition assays as well as with the FA disruption and cell rounding up occurring after ICAP-1 overexpression. These results support the idea that ICAP-1 competes with talin for binding to the β_1 cytosolic tail (Bouvard and Block, 1998; Bouvard et al., 2003). We propose that ICAP-1 can delay the talin/integrin interaction necessary for integrin activation and clustering (Calderwood, 2004; Cluzel et al., 2005; Giannone et al., 2003). This also suggests that ICAP-1 by modulating talin/integrin interaction, could limit the incorporation of β_1 integrins into FA resulting in a modification in FA dynamics. Our FACS analysis of fluorescent FN7-10 binding on cells in suspension show that the loss of ICAP-1 increases the affinity of integrin for the ligand though not as much as is achieved by incubation with either with Mn^{2+} or 9EG7 antibody. This favours the hypothesis whereby ICAP-1 could limit a state of pre-activation necessary for the following

steps of activation. Without ICAP-1, this limitation is switched off which in turn accelerates cellular mechanism such as the spreading or migration. Interestingly, when cells spread or migrate, any means of integrin activation (D/A, ICAP-1 loss, or chemical treatment) results in the same phenotype. This fits with our observation that D/A and *Icap-1* null cells share the same phenotype, but also suggests that either a threshold in integrin activation exists or that integrin activation is tightly controlled in space and time by a multi-step process implying different integrin states from preactivation to full activation of integrin as already suggested (Clark et al., 2005).

While the control of β_1 integrin high affinity state has been well characterized and is largely attributed to the interaction with the talin (Calderwood, 2004), the mechanisms restricting the β_1 integrin in a low affinity state are still unknown. Here, we show, that ICAP-1 loss results in increased β_1 integrin affinity in MEF, as previously described for osteoblasts (Bouvard et al., 2007) and that the increase of β1 integrin affinity results in faster FA turnover and in the inability of the cells to adapt their adhesive properties. This abnormal switch of β_1 integrins toward the high affinity state results in maximal cell spreading and migratory response on a coating of minimal substrate density even though no migration defect has been noticed in *Icap-1* null mice during embryogenesis. *Nevertheless, we can neither exclude the presence of a more subtle defect nor can we exclude the possibility of a migration defect in Icap-1 null mice during repair or pathogenesis.* Mice expressing a D759A mutation in β_1 locus have been recently described. In contrast to *Icap*-1-null mice, those animals do not display significant abnormalities (Czuchra et al., 2006). However, even though talin binding onto β_1 integrin is required for its full activation in both mutants, the absence of ICAP-1 expression would favor talin binding, while ICAP-1 would still limit this step in the case of the D/A mutation. Furthermore, *Icap-1* deficient mice also suffer from a strong osteoblast proliferation defect that could be integrin independent (Bouvard et al., 2007)

However our results indicate that a balance between low and high affinity integrins states is necessary for proper sensing of the ECM density, which in turn has an important consequences for migration and spreading. Cell adhesion is continually adapted in response to changes in substrate concentration and structure or to mechanical cues at the cell-matrix interface. Distinct FA and actin cytoskeleton organization and dynamics have been shown to depend on the strength cell adhesion (Gupton and Waterman-Storer, 2006). Our data provide a new insight by adding integrin affinity regulation to the molecular mechanisms controlling these different processes. Change in adhesive properties can be predicted on the basis of the

redistribution of FA. In our study, the hallmark of increased integrin affinity, corresponding to the signature of cellular adaptation to a particular matrix environment, is the redistribution of FA throughout the ventral cell surface accompanied by an expansion in their areas. Cells lacking ICAP-1 are much less capable of sensing different matrix densities; consequently maximal response is elicited by a minimum matrix density environment. Cell adaptive response and stem cells lineage specification may arise from substrate stiffness (Discher et al., 2005; Engler et al., 2006; Paszek et al., 2005). This inability to feel their environment has important consequences for *in vivo* function. Indeed, *Icap-1* null mice suffer from an important osteogenesis dysfunction resulting from reduced proliferation and delayed differentiation of the osteoblast population. *Icap-1*-deficient preosteoblasts present a condensation defect which further limits the number of progenitors that will finally differentiate into mature osteoblasts (Bouvard et al., 2007). This cell compaction defect could be a consequence of the cells inability to sense the matrix density or organization. The pronounced phenotype in osteoblasts may be due to their extraordinary need for mechanosensitivity to mediate bone formation and remodeling along with the necessity of being aware of the inherent variability in cellular response to differences in matrix density or stiffness (Leucht et al., 2007). While it is clear from previous work that β_1 integrin expression is crucial for development and tissue homeostasis, here we clearly establish that a switch between a high and low affinity integrin states is required in order to drive an integrated cell response appropriate to the ECM environment. This is achieved by specific integrin regulators such as talin, ICAP-1 and possibly other proteins that are central to the control of FA dynamics during cell adhesion.

Materials and methods

Reagents and antibodies

FN was extracted from human plasma (Albiges-Rizo et al., 1995). Rat CL was from Roche (Meylan, France) and VN from Becton Dickinson (France). Vinculin mAb (hVIN-1), actin pAb (AC40), talin mAb (8d4) and phalloidin-rhodamine were from Sigma-Aldrich. Paxillin mAb (349) was from Transduction Laboratories (BD Biosciences, Le Pont de Claix, France). Anti-human β_1 integrin mAb (4B7R) was from Neomarkers (Lab Vision Corporation, CA). Anti-mouse β_1 integrin 9EG7 and MB1.2 mAb were from Pharmingen (BD Bioscience) and generously provided by Dr. Bosco (Ontario, Canada), respectively. Anti-mouse β_3 integrin mAb was from Dr. B. Nieswandt (Wuerzburg, Germany). Tyrosinated tubulin pAb were from Laurence Lafenachère (Grenoble, France). Alexa-conjugated goat antibodies were from Molecular Probes (InVitrogen, Cergy Pontoise, France). Rabbit anti-ICAP-1 serum was raised by immunizing rabbits with purified recombinant His-tagged ICAP-1 (amino-acids 1-150) as antigen. Goat anti-mouse IgG and goat anti-rabbit IgG coupled to horse-radish peroxidase were from BioRad (Marnes-La-Coquette, France) and Jackson Immunoresearch (Europe Branch, Newmarket, UK), respectively.

Cell culture, transfection, retroviral infection and plasmid construction

Primary mouse embryonic fibroblasts (MEF) were isolated from E14.5 wild-type or *Icap-1* deficient embryos using a standard procedure. Immortalized osteoblasts from *Icap-1*$^{+/+}$, *Icap-1* null mice as well as *Icap-1* null osteoblasts rescued with *Icap-1* were generated as described previously (Bouvard et al, 2007). MEF, GD25 and osteoblast cells were cultured in D-MEM supplemented with 10% FCS (Invitrogen Gibco, Cergy-Pontoise, France) and penicillin (100 U/ml)/streptomycin (100 µg/ml) at 37°C in 5% CO_2-humidified chamber. Cells were transfected with the cDNA constructs, using Exgen 500 (Euromedex, Souffelweyersheim, France). The expression vectors were pEGFP-C1-vinculin, pEGFP-C1-paxillin (K. Nakamura), pEGFP-C1-talin (A. Huttenlocher, Madison, WI), pBabe β_1-WT, pBabe β_1(D759A), pBabe-EGFP-VASP (F. Gertler, Cambridge, MA) and pCLMFG-IRES-ICAP-1. Retroviral plasmid encoding human WT β_1 integrin or the D759A mutant was carried out using standard protocol. Briefly, a HindIII subclone fragment was used for PCR mediated mutagenesis using the QuickChange™ site directed mutagenesis kit according to the manufacturer's instructions (Stratagene, La Jolla, CA) and reinserted into the full sequence to

swap the wild-type sequence using HindIII digest. Human WT or mutant β_1 integrin was then inserted into pBabe retroviral vector using EcoRI and Xho I sites. All sequences were verified by DNA sequencing (Genome Express, Grenoble, France). β_1 integrin null GD25 cells were transfected with pBabe containing either WT or D759A β_1 integrin and selected in the presence of 1 μg/ml puromycin. For retroviral infection, cells were incubated for 24h at 37°C with either pBabe-EGFP-VASP or pCLMFG-Ires-ICAP-1 or pCLMFG-EGFP-Zyxin retrovirus containing supernant in 10% FCS DMEM and 4 μg/ml Polybrene® (Sigma Aldrich) as previously described (Bouvard et al., 2007).

Western blotting

MEF cells were lysed in RIPA buffer containing protease and phosphatase inhibitors (Roche). Proteins were separated by SDS-PAGE and transferred to PVDF membranes. Immunological detection was achieved with appropriate horseradish peroxydase-conjugated secondary antibody. Peroxydase activity was visualized by chemiluminescence (ECL, GE Healthcare, Velizy, France).

Immunofluorescence staining of cells

Cells were fixed with 4% PFA, permeabilized with 0.2% Triton X-100 and incubated with appropriate primary antibodies. After rinsing, coverslips were incubated with an appropriate Alexa-conjugated secondary antibody. The cells were mounted in Mowiol/DAPI solution and imaged on a Zeiss LSM 510 inverted confocal microscope.

Spreading assays

Cell adhesion assays were performed using 35 mm diameter hydrophobic dishes coated with various concentrations of matrix. Cells were trypsinized, treated with trypsin inhibitor (1 mg/ml, Sigma Aldrich) and incubated in serum-free DMEM/5% BSA for 1 h at 37°C. Cells were plated at a density of 2.10^4 cells per dish in 2 ml DMEM containing fibronectin-free 10% FCS. After 1.5 h incubation at 37°C, cells were photographed and scored as round or flattened using 3 fields for each experimental condition. When Mn^{2+} was supplemented, cells were treated for 10 min at 37°C in suspension with 0.5 mM $MnCl_2$ in DMEM containing fibronectin-free fetal calf serum before seeding. Alternatively, cells were treated with 10 μg/ml mAb(9EG7) for 30 min at 4°C in DMEM containing fibronectin-free FCS.

Migration assays

For transwell assays, polycarbonate membranes (8 µm pores, BD Bioscience, Falcon) were coated on both side overnight with various concentrations of matrix. After washing with PBS, chambers were transferred in 24-wells-plates containing either serum-free DMEM or DMEM plus fibronectin-free serum. Serum-starved cells were trypsinized then treated with trypsin inhibitor. 15.10^3 cells were seeded in the upper chamber in 1 ml of serum free DMEM and allowed to migrate to the underside of the membrane for 8 h. Cell migration was stopped by fixing and staining with Coomassie blue. Excess dye was removed with isopropanol/acetic acid. After removal of the non-migrating cells in the upper well, migrating cells were photographed at 10x magnification and counted using 3 randomly chosen microscopic fields.

Time lapse videomicroscopy was performed using LabTek II chambered coverglass (Nalge Nunc International, Hereford, UK) coated with various concentrations of fibronectin. Trypsinized cells were treated with trypsin inhibitor and incubated in 5% BSA for 1h at 37°C. Cells were then plated in LabTek II chambers containing DMEM supplemented with fibronectin-free serum. After 1 h spreading, cells were observed at 10X magnification using an inverted microscope (Zeiss Axiovert 100) equipped with an on-stage incubator (PeCon, Erbach, Germany). Six to eight isolated fields were arbitrary chosen and phase contrast images were taken at 4 min intervals over a period of 5 h. Cells were tracked using the position of centroids with Metamorph software (Molecular Imaging, Roper Scientific, Evry France).

FNIII7-10 binding assay and flow cytometry analysis

MEF or GD25 cells were harvested after trypsin treatment, washed in presence of trypsin inhibitor, and incubated (3.10^5 cells per sample) with 3 µM of FITC-coupled FNIII7-10 fragment (F. Coussin, Bordeaux, France) in Tyrode buffer supplemented with 1% BSA for one hour in the presence or absence of 5 mM EDTA and 5 mM EGTA. After washing with Tyrode/BSA, the cells were fixed and subjected to flow cytometry analysis using a FACScan flow cytometer (BD Bioscience). The collected data were analyzed using CellQuest software (BD Bioscience). In parallel MEF or GD25 cells were analyzed by FACS for cell surface β_1 or β_3 integrin expression using either the MB1.2 rat mAb (against mouse β_1 integrin), the 4B7R mouse mAb (against human β_1 integrin) and the anti-mouse β_3 integrin rat mAb (against mouse β3 integrin). The activation index (AI) of β_1 integrin was estimated as previously described (Bouvard et al, 2007). Each specific mean intensity fluorescence (MFI)

was calculated by subtracting the background obtained with FNIII7-10 fragment incubation in the presence of EDTA or without the primary antibody in the case of the integrin labelling. For instance for the estimation of human β_1 integrin activation (GD25 cells) : AI= ((MFI FNIII7-10)-(MFI FNIII7-10+EDTA))/(MFI 4B7R)-(MFI 4B7R control).

Nocodazole assay

Cells were serum starved for 48 h in DMEM containing 0.5% fatty acid free BSA and then treated with 10 μM nocodazole for 4 h to completely depolymerize microtubules. The drug was washed out with serum free DMEM medium containing 0.5% fatty acid free BSA, and microtubules were allowed to repolymerize for different time intervals. Cells were fixed and permeabilized before processing for immunofluorescence.

Quantification of FA area and intensity

Fixed and stained cells were imaged on Zeiss LSM 510 NLO inverted confocal and biphoton laser scanning microscope equipped with a 63x/1.4 oil-immersion plan-apochromat objective. The fluorescence of Alexa488 and Alexa546 was excited with 488 or 543 nm wavelengths and detected in confocal mode. The Alexa350 fluorescence was induced by two-photon absorption at 720 nm using the fs Ti:Sa laser (Tsunami, Spectra-Physics, Every, France) . Neither signal saturation nor significant photobleaching was induced during image acquisition in either detection channel.

The images were manually thresholded and FA were automatically selected using Metamorph software within the predefined regions of the cell. The number and areas of FA and the average fluorescence intensities of β_1, β_3 integrin, vinculin and paxillin in FA were quantified.

Time-lapse videomicroscopy and Quantification of FA dynamics

Time-lapse recordings were assessed either on MEF cells expressing EGFP-paxillin or EGFP-VASP or EGFP-vinculin on GD25 cells expressing EGFP-Zyxin. Cells were cultured in fibronectin-free FCS DMEM on LabTekII chambers previously coated with indicated concentrations of matrix. Living cells were maintained at 37°C in 5% CO_2 atmosphere under a Zeiss Axiovert 200M inverted microscope equipped with a motorized stage, cooled CCD camera and a LCI Plan Apochromat 63x/1.2 water immersion objective. In order to minimize the possible photobleaching and light-induced cell damage, the excitation light of 100W Hg lamp was reduced to 30% with a FluoArc system and additionally attenuated with ND75

filter. Fifteen isolated cells were randomly chosen for each experimental condition and 10 to 15 control WT cells were recorded simultaneously. Images were acquired looping all stage positions at 4 min intervals over 6 h. The turn-over of FA located at the cell front was quantified using Metamorph software. Briefly, the adhesion area was outlined on the raw images during steady state, then adhesion was manually followed from its nucleation and the mean fluorescence intensity in the same area was measured subtracting the background value. Four parameters of adhesion turnover were determined: the total lifetime, the period of steady state and the rates of assembly and disassembly.

Fluorescence recovery after photobleaching (FRAP)

MEF cells transiently expressing EGFP-talin or EGFP-vinculin were cultured on LabTek II chambers (Nalge Nunc International) previously coated with either 20 µg/ml fibronectin or 5 µg/ml VN. FRAP experiments were performed with a LSM510 confocal microscope equipped with the on-stage incubator. One individual FA per cell located at the leading edge was processed by FRAP. EGFP fluorescence in adhesion area was eliminated by 100 bleach cycles at 100% intensity of the 488 nm argon laser. The fluorescence recovery was then sampled with low laser power (2-3%) each minute for 15-20 min. The recovery curves were obtained using Metamorph software by measuring the average fluorescence intensity in the bleached region and correcting it to the overall image photobleaching. The corrected curve was adjusted with Kaleidagraph software (SynergySoftware, Reading, PA) using the monoexponential fit. The characteristic recovery time, τ was the average of at least 20 individual FA.

Aknowledgements

We would like to thank members of the laboratory for all their input and helpful discussions. We thank E. Planus, J. Torbet, K. Sadoul for critical reading of the manuscript. We thank G. Chevalier for technical assistance and A. Stuani for imaging assistance. This work was supported by a grant from the Ligue Nationale Contre le Cancer, the Association de Recherche pour le Cancer, ARECA, and the Région Rhône-Alpes. A. M.-F. was supported by a fellowship from the Ministère de l'Education Nationale, de la Recherche et de la Technologie.

Abbreviations used in this paper:

ECM, extracellular matrix; CL, type I collagen; FA, focal adhesion; FN, fibronectin; VN, vitronectin; WT, wild type; MEF Mouse, Embryonic Fibroblasts.

References

Albiges-Rizo, C., P. Frachet, and M.R. Block. 1995. Down regulation of talin alters cell adhesion and the processing of the alpha 5 beta 1 integrin. *J Cell Sci*. 108:3317-29.

Bennett, J.S. 2005. Structure and function of the platelet integrin alphaIIbbeta3. *J Clin Invest*. 115:3363-9.

Bershadsky, A.D., N.Q. Balaban, and B. Geiger. 2003. Adhesion-dependent cell mechanosensitivity. *Annu Rev Cell Dev Biol*. 19:677-95.

Bhatt, A., I. Kaverina, C. Otey, and A. Huttenlocher. 2002. Regulation of focal complex composition and disassembly by the calcium-dependent protease calpain. *J Cell Sci*. 115:3415-25.

Bouvard, D., A. Aszodi, G. Kostka, M.R. Block, C. Albiges-Rizo, and R. Fassler. 2007. Defective osteoblast function in ICAP-1-deficient mice. *Development*.

Bouvard, D., and M.R. Block. 1998. Calcium/calmodulin-dependent protein kinase II controls integrin alpha5beta1-mediated cell adhesion through the integrin cytoplasmic domain associated protein-1alpha. *Biochem Biophys Res Commun*. 252:46-50.

Bouvard, D., L. Vignoud, S. Dupe-Manet, N. Abed, H.N. Fournier, C. Vincent-Monegat, S.F. Retta, R. Fassler, and M.R. Block. 2003. Disruption of focal adhesions by integrin cytoplasmic domain-associated protein-1 alpha. *J Biol Chem*. 278:6567-74.

Calderwood, D.A. 2004. Integrin activation. *J Cell Sci*. 117:657-66.

Calderwood, D.A., B. Yan, J.M. de Pereda, B.G. Alvarez, Y. Fujioka, R.C. Liddington, and M.H. Ginsberg. 2002. The phosphotyrosine binding-like domain of talin activates integrins. *J Biol Chem*. 277:21749-58.

Chang, D.D., B.Q. Hoang, J. Liu, and T.A. Springer. 2002. Molecular basis for interaction between Icap1 alpha PTB domain and beta 1 integrin. *J Biol Chem*. 277:8140-5.

Chang, D.D., C. Wong, H. Smith, and J. Liu. 1997. ICAP-1, a novel beta1 integrin cytoplasmic domain-associated protein, binds to a conserved and functionally important NPXY sequence motif of beta1 integrin. *J Cell Biol*. 138:1149-57.

Chen, C.S., J. Tan, and J. Tien. 2004. Mechanotransduction at cell-matrix and cell-cell contacts. *Annu Rev Biomed Eng*. 6:275-302.

Clark, K., R. Pankov, M.A. Travis, J.A. Askari, A.P. Mould, S.E. Craig, P. Newham, K.M. Yamada, and M.J. Humphries. 2005. A specific alpha5beta1-integrin conformation promotes directional integrin translocation and fibronectin matrix formation. *J Cell Sci*. 118:291-300.

Cluzel, C., F. Saltel, J. Lussi, F. Paulhe, B.A. Imhof, and B. Wehrle-Haller. 2005. The mechanisms and dynamics of (alpha)v(beta)3 integrin clustering in living cells. *J Cell Biol*. 171:383-92.

Czuchra, A., H. Meyer, K.R. Legate, C. Brakebusch, and R. Fassler. 2006. Genetic analysis of beta1 integrin "activation motifs" in mice. *J Cell Biol*. 174:889-99.

Discher, D.E., P. Janmey, and Y.L. Wang. 2005. Tissue cells feel and respond to the stiffness of their substrate. *Science*. 310:1139-43.

Engler, A.J., S. Sen, H.L. Sweeney, and D.E. Discher. 2006. Matrix elasticity directs stem cell lineage specification. *Cell*. 126:677-89.

Ezratty, E.J., M.A. Partridge, and G.G. Gundersen. 2005. Microtubule-induced focal adhesion disassembly is mediated by dynamin and focal adhesion kinase. *Nat Cell Biol*. 7:581-90.

Fournier, H.N., S. Dupe-Manet, D. Bouvard, M.L. Lacombe, C. Marie, M.R. Block, and C. Albiges-Rizo. 2002. Integrin cytoplasmic domain-associated protein 1alpha (ICAP-1alpha) interacts directly with the metastasis suppressor nm23-H2, and both proteins

are targeted to newly formed cell adhesion sites upon integrin engagement. *J Biol Chem*. 277:20895-902.

Franco, S.J., M.A. Rodgers, B.J. Perrin, J. Han, D.A. Bennin, D.R. Critchley, and A. Huttenlocher. 2004. Calpain-mediated proteolysis of talin regulates adhesion dynamics. *Nat Cell Biol*. 6:977-83.

Giannone, G., G. Jiang, D.H. Sutton, D.R. Critchley, and M.P. Sheetz. 2003. Talin1 is critical for force-dependent reinforcement of initial integrin-cytoskeleton bonds but not tyrosine kinase activation. *J Cell Biol*. 163:409-19.

Ginsberg, M.H., A. Partridge, and S.J. Shattil. 2005. Integrin regulation. *Curr Opin Cell Biol*. 17:509-16.

Gupton, S.L., and C.M. Waterman-Storer. 2006. Spatiotemporal Feedback between Actomyosin and Focal-Adhesion Systems Optimizes Rapid Cell Migration. *Cell*. 125:1361-74.

Han, J., C.J. Lim, N. Watanabe, A. Soriani, B. Ratnikov, D.A. Calderwood, W. Puzon-McLaughlin, E.M. Lafuente, V.A. Boussiotis, S.J. Shattil, and M.H. Ginsberg. 2006. Reconstructing and deconstructing agonist-induced activation of integrin alphaIIbbeta3. *Curr Biol*. 16:1796-806.

Hughes, P.E., F. Diaz-Gonzalez, L. Leong, C. Wu, J.A. McDonald, S.J. Shattil, and M.H. Ginsberg. 1996. Breaking the integrin hinge. A defined structural constraint regulates integrin signaling. *J Biol Chem*. 271:6571-4.

Hynes, R.O. 2002. Integrins: bidirectional, allosteric signaling machines. *Cell*. 110:673-87.

Ingber, D.E. 2003. Mechanosensation through integrins: cells act locally but think globally. *Proc Natl Acad Sci U S A*. 100:1472-4.

Jiang, G., G. Giannone, D.R. Critchley, E. Fukumoto, and M.P. Sheetz. 2003. Two-piconewton slip bond between fibronectin and the cytoskeleton depends on talin. *Nature*. 424:334-7.

Kaverina, I., O. Krylyshkina, and J.V. Small. 1999. Microtubule targeting of substrate contacts promotes their relaxation and dissociation. *J Cell Biol*. 146:1033-44.

Leucht, P., J.B. Kim, J.A. Currey, J. Brunski, and J.A. Helms. 2007. FAK-Mediated Mechanotransduction in Skeletal Regeneration. *PLoS ONE*. 2:e390.

Liddington, R.C., and M.H. Ginsberg. 2002. Integrin activation takes shape. *J Cell Biol*. 158:833-9.

Luo, B.H., T.A. Springer, and J. Takagi. 2004. A specific interface between integrin transmembrane helices and affinity for ligand. *PLoS Biol*. 2:e153.

Martel, V., C. Racaud-Sultan, S. Dupe, C. Marie, F. Paulhe, A. Galmiche, M.R. Block, and C. Albiges-Rizo. 2001. Conformation, localization, and integrin binding of talin depend on its interaction with phosphoinositides. *J Biol Chem*. 276:21217-27.

Partridge, A.W., S. Liu, S. Kim, J.U. Bowie, and M.H. Ginsberg. 2005. Transmembrane domain helix packing stabilizes integrin alphaIIbbeta3 in the low affinity state. *J Biol Chem*. 280:7294-300.

Paszek, M.J., N. Zahir, K.R. Johnson, J.N. Lakins, G.I. Rozenberg, A. Gefen, C.A. Reinhart-King, S.S. Margulies, M. Dembo, D. Boettiger, D.A. Hammer, and V.M. Weaver. 2005. Tensional homeostasis and the malignant phenotype. *Cancer Cell*. 8:241-54.

Priddle, H., L. Hemmings, S. Monkley, A. Woods, B. Patel, D. Sutton, G.A. Dunn, D. Zicha, and D.R. Critchley. 1998. Disruption of the talin gene compromises focal adhesion assembly in undifferentiated but not differentiated embryonic stem cells. *J Cell Biol*. 142:1121-33.

Raftopoulou, M., and A. Hall. 2004. Cell migration: Rho GTPases lead the way. *Dev Biol*. 265:23-32.

Sakai, T., Q. Zhang, R. Fassler, and D.F. Mosher. 1998. Modulation of beta1A integrin functions by tyrosine residues in the beta1 cytoplasmic domain. *J Cell Biol*. 141:527-38.

Schober, M., S. Raghavan, M. Nikolova, L. Polak, H.A. Pasolli, H.E. Beggs, L.F. Reichardt, and E. Fuchs. 2007. Focal adhesion kinase modulates tension signaling to control actin and focal adhesion dynamics. *J Cell Biol*. 176:667-80.

Tadokoro, S., S.J. Shattil, K. Eto, V. Tai, R.C. Liddington, J.M. de Pereda, M.H. Ginsberg, and D.A. Calderwood. 2003. Talin binding to integrin beta tails: a final common step in integrin activation. *Science*. 302:103-6.

Takagi, J., and T.A. Springer. 2002. Integrin activation and structural rearrangement. *Immunol Rev*. 186:141-63.

Vinogradova, O., J. Vaynberg, X. Kong, T.A. Haas, E.F. Plow, and J. Qin. 2004. Membrane-mediated structural transitions at the cytoplasmic face during integrin activation. *Proc Natl Acad Sci U S A*. 101:4094-9.

Webb, D.J., K. Donais, L.A. Whitmore, S.M. Thomas, C.E. Turner, J.T. Parsons, and A.F. Horwitz. 2004. FAK-Src signalling through paxillin, ERK and MLCK regulates adhesion disassembly. *Nat Cell Biol*. 6:154-61.

Zaidel-Bar, R., R. Milo, Z. Kam, and B. Geiger. 2007. A paxillin tyrosine phosphorylation switch regulates the assembly and form of cell-matrix adhesions. *J Cell Sci*. 120:137-48.

Zhang, X.A., and M.E. Hemler. 1999. Interaction of the integrin beta1 cytoplasmic domain with ICAP-1 protein. *J Biol Chem*. 274:11-9.

Figures legends

Figure 1: ICAP-1 loss induces the central redistribution of FA and increases β_1 integrin clustering.

(A -B) Confocal images obtained with *Icap-1*$^{+/+}$, and *Icap-1*$^{-/-}$ MEF cells **(A)** or *Icap-1*$^{+/+}$, *Icap-1*$^{-/-}$ and *Icap-1*^{rescue} osteoblasts **(B)**. Cells were cultured overnight on 10µg/ml FN, and processed for immunofluorescence labelling to visualize β_1 integrin (9EG7), paxillin and vinculin. Note the increased number of FA at the cell surface underlying the main cell body in *Icap-1*$^{-/-}$ MEF cells and osteoblasts and the exclusive peripheral distribution of adhesion sites in rescued osteoblasts. Bar is 20 µm. **(C-D)** *Icap-1*$^{+/+}$and *Icap-1*$^{-/-}$ MEF cells were plated on 10µg/ml FN and allowed to spread for 2 hours. Immunostaining was processed to visualize vinculin, paxillin, β_1 or β_3 integrins. Confocal images of each cell type were acquired and subjected to image analysis with Metamorph software. **(C)** The average surface of β_3 or β_1 integrins containing FA (top histogram) and the mean fluorescence intensity of β_1 and β_3 integrins in vinculin stained FA (bottom histogram) were measured in *Icap-1*$^{+/+}$ and *Icap-1*$^{-/-}$ MEF cells. Right images show β1 and β3 integrin containing focal adhesions in both cell types **(D)** The ratio of the mean intensities of vinculin, paxillin or talin containing FA normalized to β_1 integrin was then estimated. Experiments were performed in duplicate and at least 20 cells were analyzed for each immunostaining. Error bars indicate SD.

Figure 2: ICAP-1 loss shifts the optimum substrate concentration for migration and facilitated adhesion.

(A) The migration of *Icap-1*$^{+/+}$ and *Icap-1*$^{-/-}$ MEF cells was studied in a random chemotactic transwell assay. Cells were seeded in transwell chambers coated on both sides with increasing concentrations of FN or CL ranging from 0.5 to 20 µg/ml. After 8 h cell migration was stopped and cells were stained and fixed by coomassie blue. The cells localized on the underside of the membrane were counted and the number of cells per field was used to quantify cell migration. Error bars indicate SD of at least 3 individual experiments. **(B)** The migration speed of *Icap-1*$^{+/+}$ and *Icap-1*$^{-/-}$ MEF cells was determined on various FN concentrations by using time-lapse phase contrast video-microscopy and cell tracking with Metamorph software. 20 to 40 cells were photographed for each experimental condition at 4 min intervals over an 8 hours period. Error bars is SD from 3 separate experiments. The maximal migration speed was used to set up 100 % for each cell type. **(C-D)** Spreading assay of *Icap-1*$^{+/+}$ and *Icap-1*$^{-/-}$ MEF cells **(C)** as well as *Icap-1*$^{+/+}$, *Icap-1*$^{-/-}$ and *Icap-1*^{rescue}

osteoblasts **(D)** on increasing substrate densities. Cells were seeded on various concentrations of FN or CL coated surfaces and were allowed to spread for 1h30. Round and flattened cells were counted and spread cells were expressed as percent of total cell number. Each data point represents the average of at least three separate experiments and error bars are SD. *P ≤ 0.03.

Figure 3: ICAP-1 loss induces a faster recruitment of talin into FA.

Icap-1$^{+/+}$ and *Icap-1*$^{-/-}$ MEF cells were seeded in Lab-TekII chambers coated with either 20µg/ml FN **(A)** or 5µg/ml VN **(B)** and allowed to spread for 12h. After transfection, both cell types expressing either EGFP-talin or EGFP-vinculin were subjected to FRAP experiments. Photobleaching was performed on manually delimited individual FA localized at the edge of cells. EGFP fluorescence recovery was measured at 1 min intervals over a 15-20 min period and the characteristic recovery time (τ) of each FA protein was estimated. At least 20 FA were recorded for both cell types. Error bars indicate SD. The shorter recovery time τ of EGFP-talin in *Icap-1*$^{-/-}$ cells indicates a higher mobility of this protein e.g. its faster recruitment into FA. *P≤ 0.01.

Figure 4: ICAP-1 modulates FA turnover by controlling its assembly rate.

(A) Confocal images of *Icap-1*$^{+/+}$ and *Icap-1*$^{-/-}$ MEF cells either immunostained to visualize endogenous paxillin or transfected to express EGFP-VASP. Bar : 20µm. **(B-F)** *Icap-1*$^{+/+}$ and *Icap-1*$^{-/-}$ MEF cells expressing either EGFP-paxillin, EGFP-vinculin or EGFP-VASP were allowed to spread on 1 µg/ml FN for 12 h in a Lab-TekII chamber. Then, cells were imaged by time-lapse video-microscopy at 4 min intervals for 6 h. The resulting data were subjected to image analysis using Metamorph software. The mean pixel intensity of a defined FA was followed overtime and this analysis allowed the four parameters of FA turnover to be measured: The measurement of the positive **(B)** or negative **(C)** variations per minute of the mean pixel intensity reflecting the assembly and the disassembly rates respectively for each individual FA in *Icap-1*$^{+/+}$ and *Icap-1*$^{-/-}$ cells, **(D)** the time during which the mean pixel intensity did not fluctuate corresponds to the FA steady state, and **(E)** the total time during which EGFP fused adhesion proteins remain localized in a FA represents the FA lifetime. At least 20 cells of both cell types were recorded. Each point represents an individual FA, the horizontal bars are the average of all FA. **(F)** These four parameters were compiled in a schematic model of FA turnover in *Icap-1*$^{+/+}$ and *Icap-1*$^{-/-}$ cells. The higher FA assembly rate in *Icap-1*$^{-/-}$ cells and the reduced steady state duration induced the shortening of FA lifetime.*P < 0.05. **P < 10^4. ***P < 10^6.

Figure 5: ICAP-1 loss induces *de novo* FA formation upon nocodazole treatment.

(A) *Icap-1*$^{+/+}$ and *Icap-1*$^{-/-}$ MEF cells were either untreated or treated with 10µM nocodazole for 4h or treated with 10µM nocodazole for 4h followed by the drug washout for 60 and 90 min and then fixed. FA and microtubules were visualized by immunostaining of vinculin (green) and tyrosinated tubulin (red) and imaged using confocal microscopy. Scale bar is 20 µm. **(B)** Image quantification of vinculin stained *Icap-1*$^{+/+}$ and *Icap-1*$^{-/-}$ cells. Peripheral (left panels) or central (right panels) FA number per cell was counted (top panels) at each indicated steps of the nocodazole assay and their corresponding mean surface (bottom panels) was quantified. 20 cells were analyzed for each experimental condition and error bars indicate SD.

Figure 6: β_1 integrin activation induces a spreading phenotype similar to ICAP-1 loss.

(A) The β_1 integrin activation state in *Icap-1*$^{+/+}$ and *Icap-1*$^{-/-}$ cells was determined by a FNIII7-10 binding assay which measures the ability of integrins to bind FITC-conjugated FNIII7-10 by flow cytometry analysis as described under Materials and Methods. The activation index of integrin was expressed relative to the cell surface expression of β_1 integrin as previously estimated by flow cytometry using MB1.2 mAb. **(B-C)** Spreading assays of *Icap-1*$^{+/+}$ and *Icap-1*$^{-/-}$ MEF cells with or without treatment using either 0.5 mM $MnCl_2$ **(B)** or with 10µg/ml 9EG7 mAb **(C)**. Cells were first treated in suspension then plated in a dose dependent manner on FN. Cell spreading was measured as described previously in fig. 2C. Error bars indicate SD from 3 independent experiments.

Figure 7: Activated β_1 integrin increases FA turnover and promotes cell migration and spreading at low matrix density.

The human WT β_1 integrin chains or activated mutant (D759A) were stably expressed in β_1 integrin deficient GD25 cells and their adhesive properties were analyzed. **(A)** The integrin affinity state for both cell types was measured with the FNIII7-10 binding assay as described in fig. 6A. **(B)** Confocal images of GD25/WT and D759A β_1 cells spread on 10µg/ml FN and immunostained to visualize β_1 integrin, paxillin and F-actin. β_1 integrin was labeled with the 4B7R mAb which recognizes human β_1 integrin chain. Bar: 20µm. **(C)** Cell spreading and migration assays of GD25/ WT and D759A β_1 cells. Spreading of both cells types with or without 0.5 mM $MnCl_2$ treatment was measured as described in fig. 6B. Migration of both cells types was analyzed using time-lapse phase contrast video-microscopy and cell tracking

as described in fig. 2B. **(D)** GD25 cells stably expressing EGFP-zyxin and either WT β_1 or D759A integrin were spread on 5µg/ml FN and monitored by time-lapse videomicroscopy at 4 min intervals for 6 h. FA dynamics were assessed as described in fig. 4. Four parameters for FA located at the leading edge of migrating cells were measured: assembly and disassembly speed, steady state duration, and lifetime. *$P<10^5$.

Figure 8: ICAP-1 loss decreases matrix density sensing.

(A) *Icap-1*$^{+/+}$ and *Icap-1*$^{-/-}$ MEF cells were spread on various FN concentrations and immunostained to visualize vinculin and β_1 integrin (9EG7). Images were taken with a confocal microscope. Bar: 20 µm. **(B)** The number of vinculin stained FA/cell and **(C)** the mean fluorescence intensity of β_1 integrin staining within FA were measured for each FN concentration. 50 cells were analyzed for each experimental condition and error bars indicate SD. **(D-E)** EGFP-paxillin expressing *Icap-1*$^{+/+}$ and *Icap-1*$^{-/-}$ MEF cells were spread on FN at concentrations ranging from 1 to 50 µg/ml and recorded by time-lapse video-microscopy at 4 min intervals for 6 h. FA turnover was quantified as previously described in fig. 4: The rates of FA assembly and disassembly were determined as well as the duration of the steady state and total lifetime at three different FN densities (1µg/ml, 10µg/ml, 50µg/ml). Data from at least 20 cells per experimental condition were recorded. Each point represents a single FA and the horizontal bar shows the average of all FA. These parameters were compiled in a schematic model of FA turnover in *Icap-1*$^{+/+}$ and *Icap-1*$^{-/-}$ cells. Adhesion site turnover displays different behaviors depending on matrix density. Note the appearance of a steady state plateau in both cell types at high FN concentrations without any change in FA lifetime.

Figure S1: ICAP-1 loss induces no change in the distribution of β_3 integrin containing FA and in the expression of adhesion proteins.

(A) Confocal images of *Icap-1*$^{+/+}$ and *Icap-1*$^{-/-}$ MEF cells. Cells were cultured overnight on 1µg/ml FN and processed for immunostaining to visualize β3 integrin and vinculin. **(B)** ICAP-1 and FA proteins expression in *Icap-1*$^{+/+}$ and *Icap-1*$^{-/-}$ MEF cells. An equal amount of protein from cell lysates in RIPA was subjected to Western blotting analysis using either anti-ICAP-1 pAb, or anti-talin, or anti-vinculin or anti-paxillin mAb. The same membrane has been blotted with anti-actin mAb in order to control loading. **(C)** Cell surface analysis of β_1 and β_3 integrins expression on *Icap-1*$^{+/+}$ and *Icap-1*$^{-/-}$ MEF cells estimated by flow cytometry. Left panel, *Icap-1*$^{+/+}$ (fill dark line and red) or *Icap-1*$^{-/-}$ cells (dashed line and blue) were

stained with control Ab (dark) or anti β_1 MB1.2 mAb. Right panel, *Icap-1*$^{+/+}$ (fill dark line and blue) or *Icap-1*$^{-/-}$ (dashed line and red) cells were stained with control antibody (dark) or anti β_3 rat mAb.

Figure S2: *Icap-1*$^{+/+}$and *Icap-1*^{rescue} MEF cells display similar spreading and migration velocity.

(A) Spreading assay of *Icap-1*$^{+/+}$, *Icap-1*$^{-/-}$ and *Icap-1*^{rescue} MEF cells on increasing FN substrate densities. Cells were seeded on various concentrations of FN coated surfaces and were allowed to spread for 1 hour. Round and flattened cells were counted and spread cells were expressed as percent of total cell number. Each point represents the average of two separate experiments and error bars are SD. *P<0.05. **(B)** The migration speed of *Icap-1*$^{+/+}$, *Icap-1*$^{-/-}$ and *Icap-1*^{rescue} MEF cells was determined on various FN concentrations using time-lapse phase contrast video-microscopy and cell tracking with Metamorph software. 20 to 40 cells were photographed for each experimental condition at 4 min intervals over an 8 hours period. Error bars are SD from 3 separate experiments. The maximal migration speed was used to set up 100 % for each cell type.

Figure S3: Migration, spreading and FA dynamics of *Icap-1*$^{-/-}$ MEF cells were not affected on VN.

(A) The migration of *Icap-1*$^{+/+}$ and *Icap-1*$^{-/-}$ MEF cells was studied using a random chemotactic transwell assay with both sides of chambers coated with increasing concentrations of VN. Error bars indicate SD of at least 3 individual experiments. **(B)** The spreading of *Icap-1*$^{+/+}$ and *Icap-1*$^{-/-}$ MEF cells on various concentrations of VN and treated or not with 0.5 mM $MnCl_2$ was measured. Each point represents the average of at least three separate experiments and error bars are SD. **(C)** EGFP-paxillin expressing *Icap-1*$^{+/+}$ and *Icap-1*$^{-/-}$ MEF cells were spread on 1µg/ml VN and recorded by time-lapse video-microscopy at 4 min intervals for 6 h. The rates of formation and disassembly as well as FA steady state and lifetime were determined as previously described in fig. 4. At least 20 cells per experimental condition were recorded. Each data point represents one FA and the horizontal bar shows the average of all FA with error bars indicating the SD.

Figure S4: β_1 integrin activation in *Icap-1*$^{+/+}$ and *Icap-1*^{rescue} cells induces a spreading phenotype similar to *Icap-1*$^{-/-}$ cells.

Spreading assays of *Icap-1*$^{+/+}$ and *Icap-1*$^{-/-}$ MEF cells **(A)** and *Icap-1*$^{+/+}$, *Icap-1*$^{-/-}$ and *Icap-1*^{rescue} osteoblasts **(B-C)** with or without treatment using either 0.5 mM $MnCl_2$ **(A,B)** or with 10µg/ml 9EG7 mAb **(C)**. Cells were treated in suspension after plated in a dose dependent manner on either FN or CL. Cell spreading was measured as described previously in fig. 2C. Error bars indicate SD from 3 independent experiments.

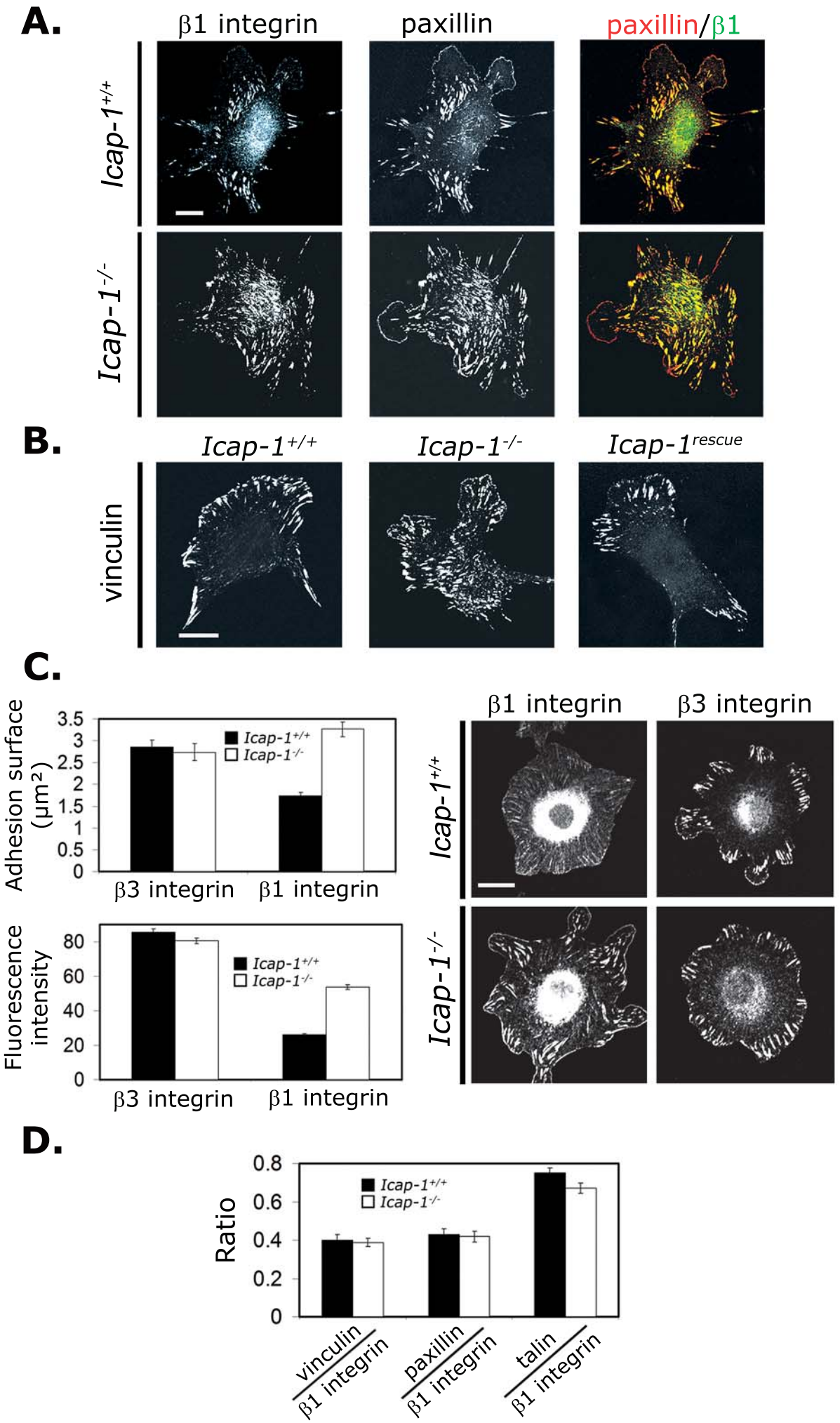

Figure 1. **Millon Fremillon A. et al,**

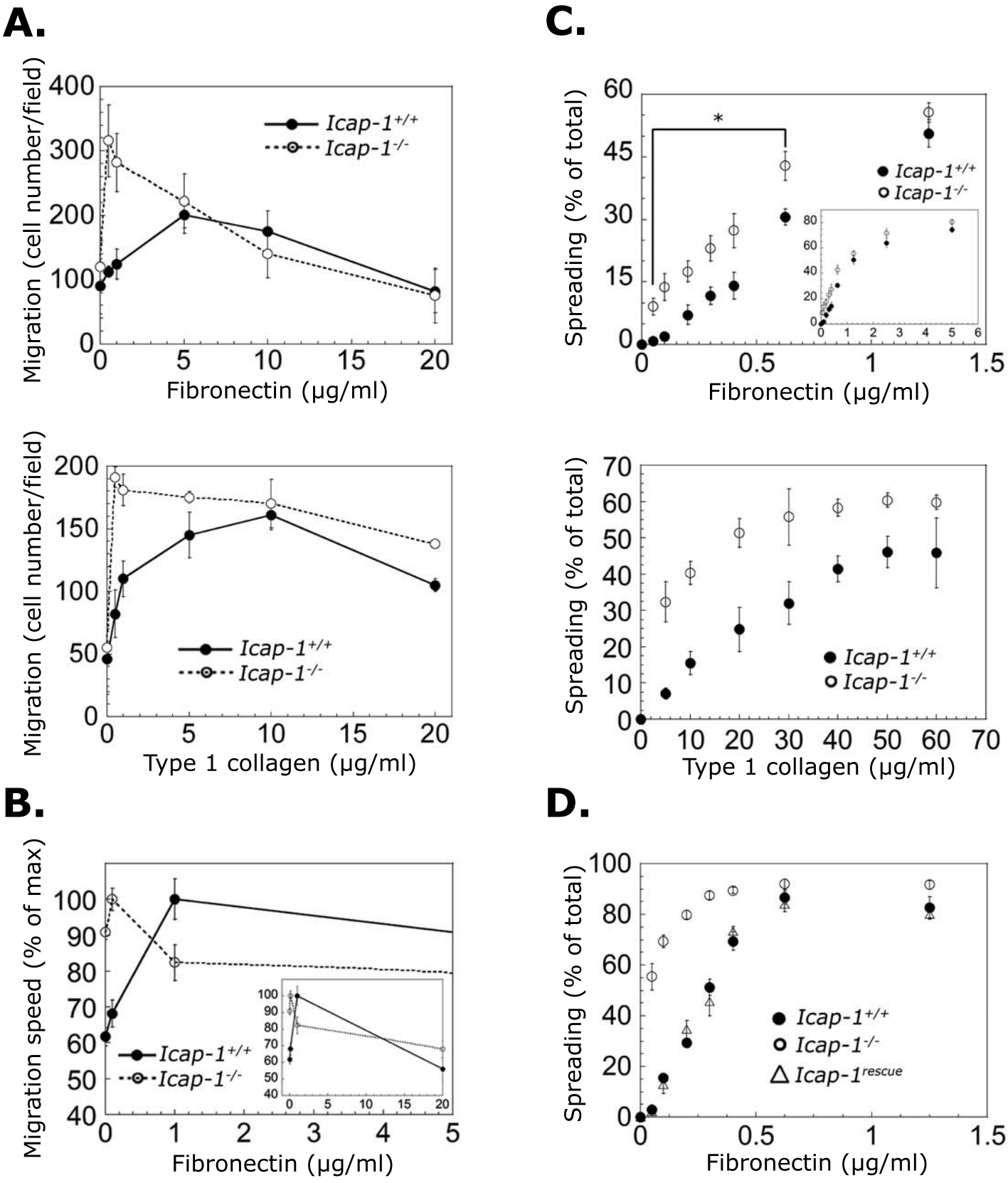

Figure 2. Millon Fremillon A. et al,

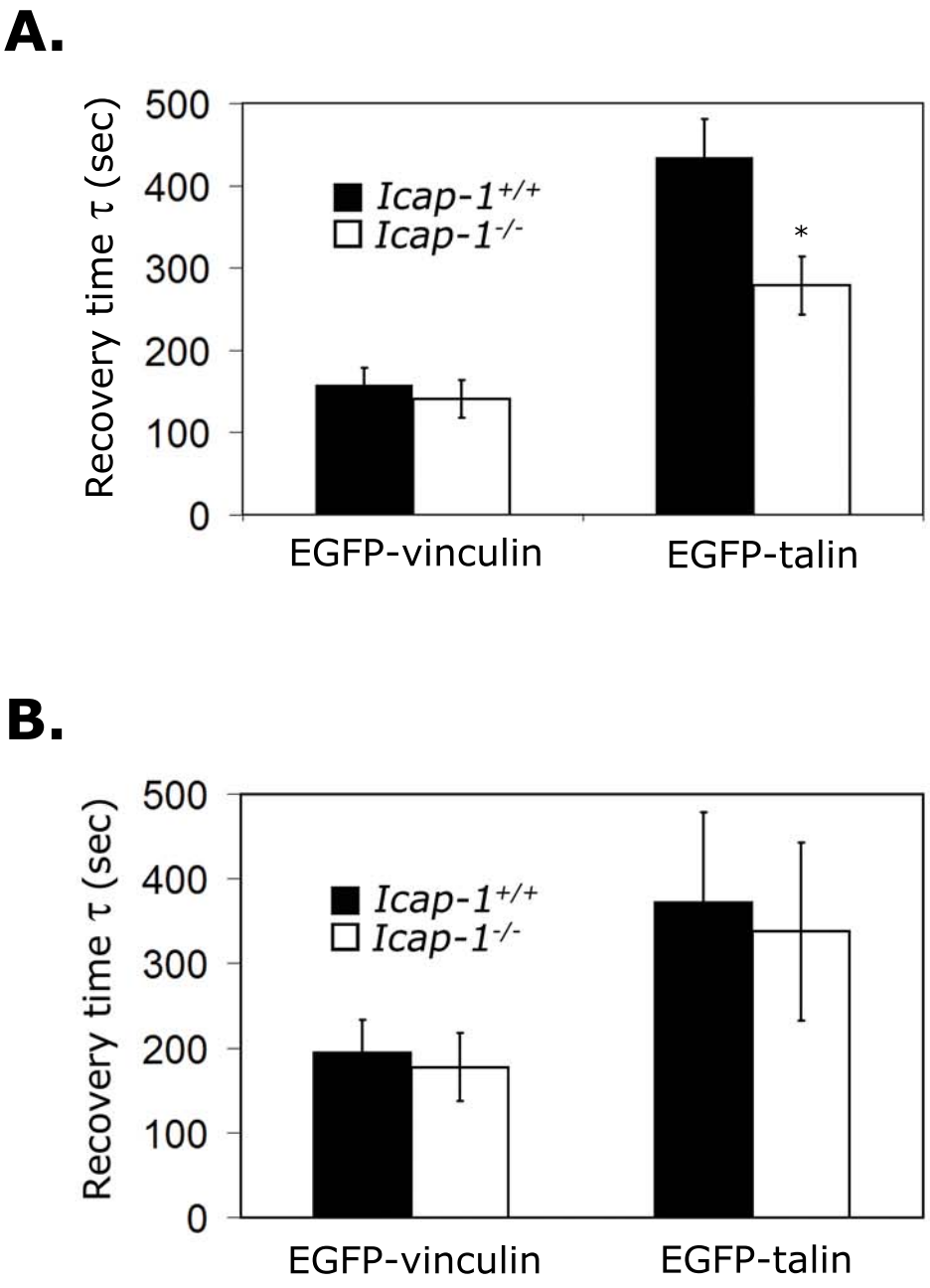

Figure 3. **Millon Fremillon A. et al,**

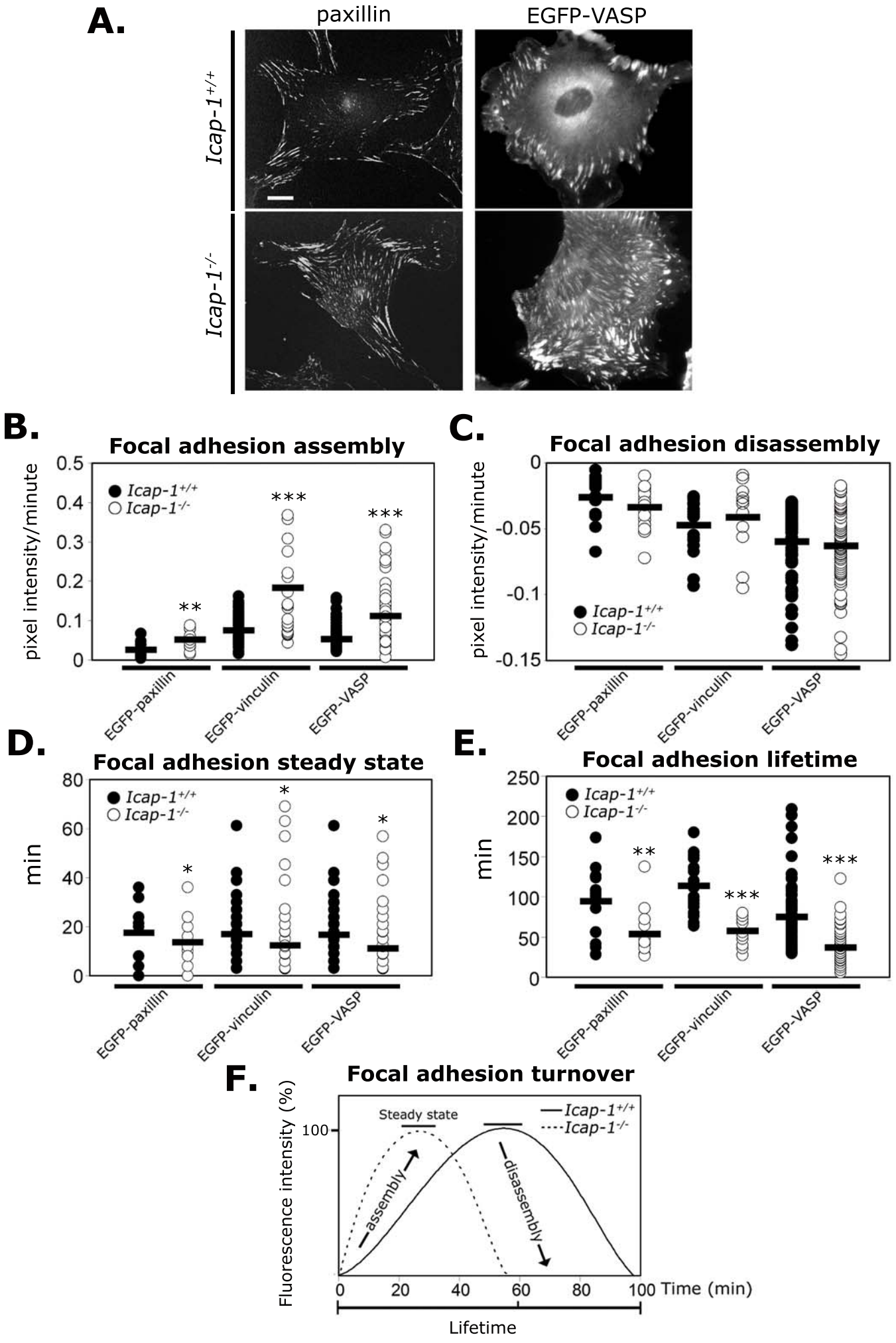

Figure 4. **Millon Fremillon A. et al,**

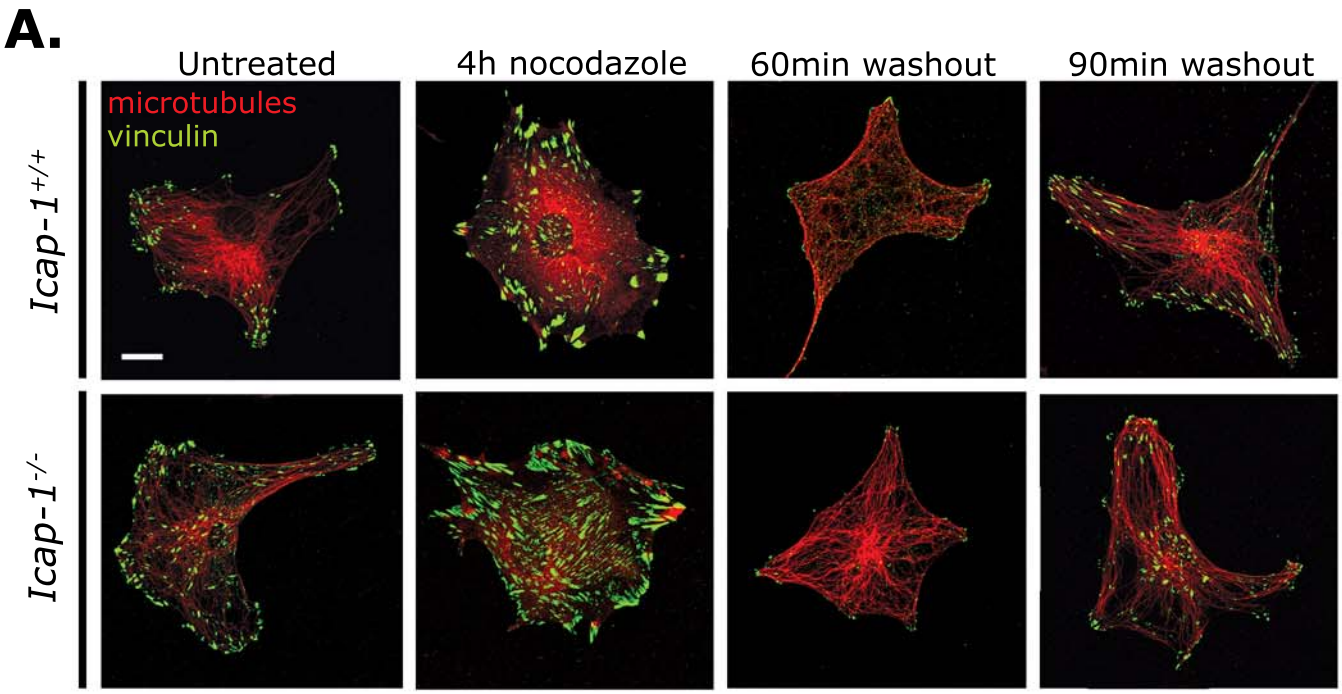

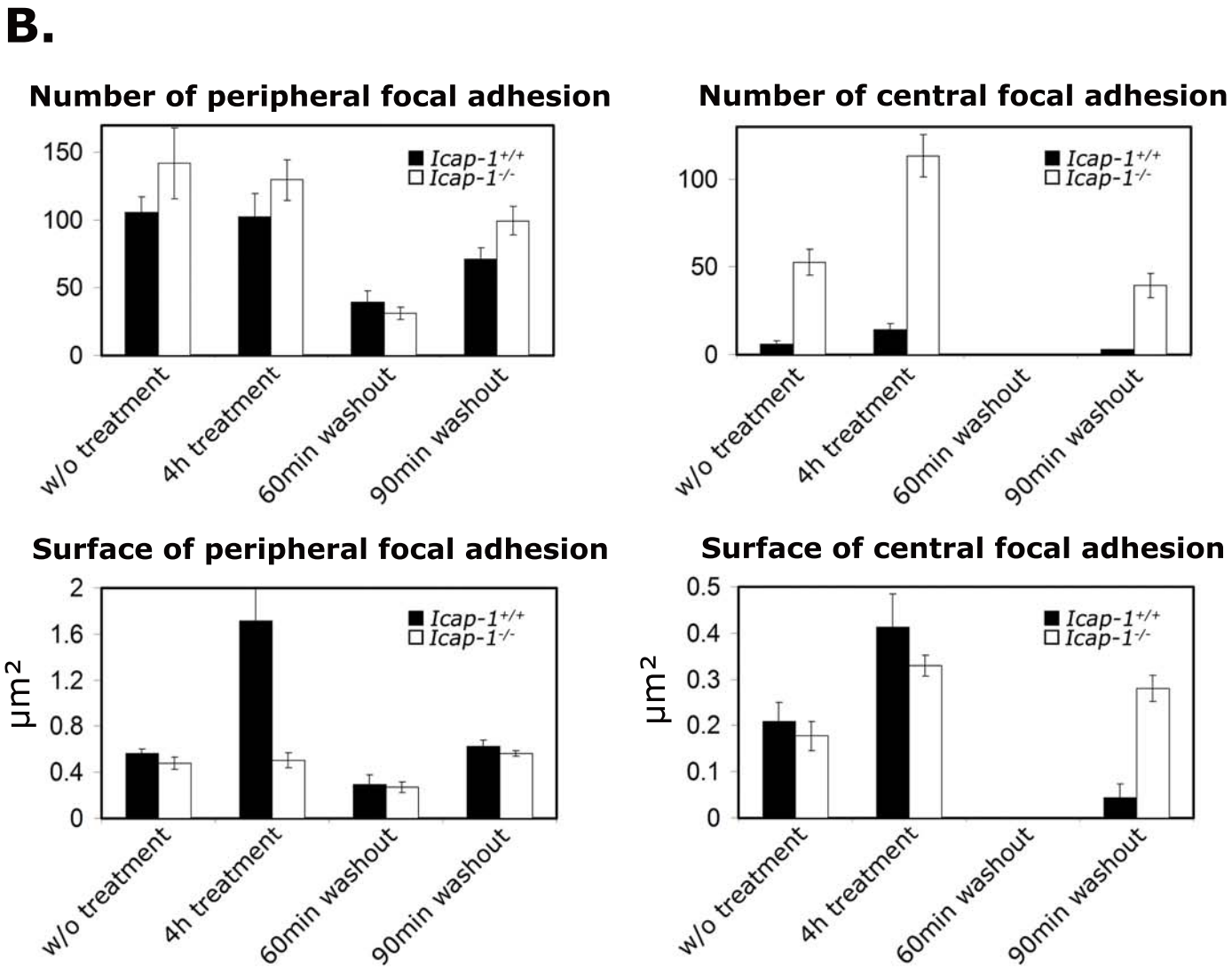

Figure 5. **Millon Fremillon A. et al,**

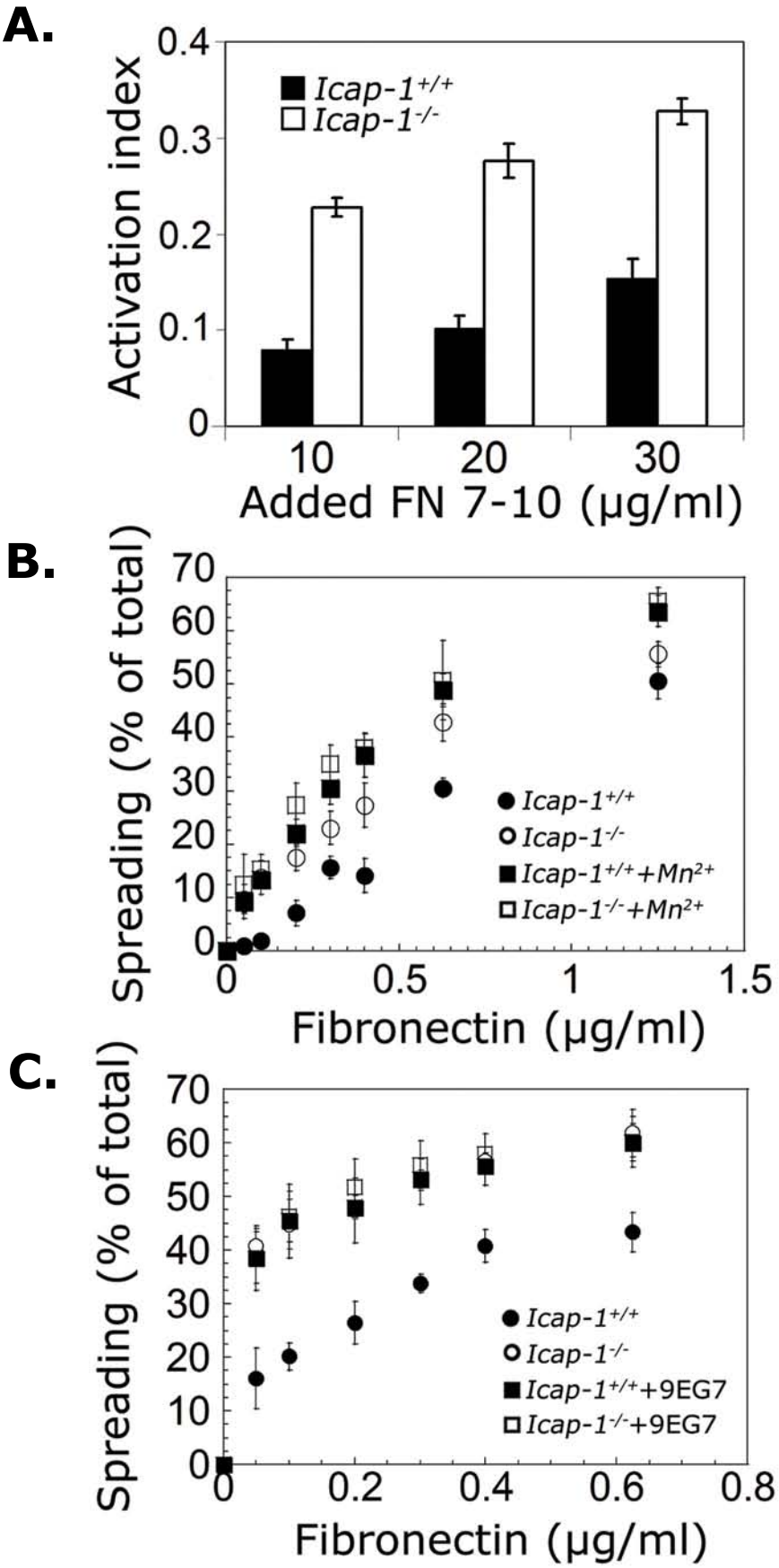

Figure 6. **Millon Fremillon A. et al,**

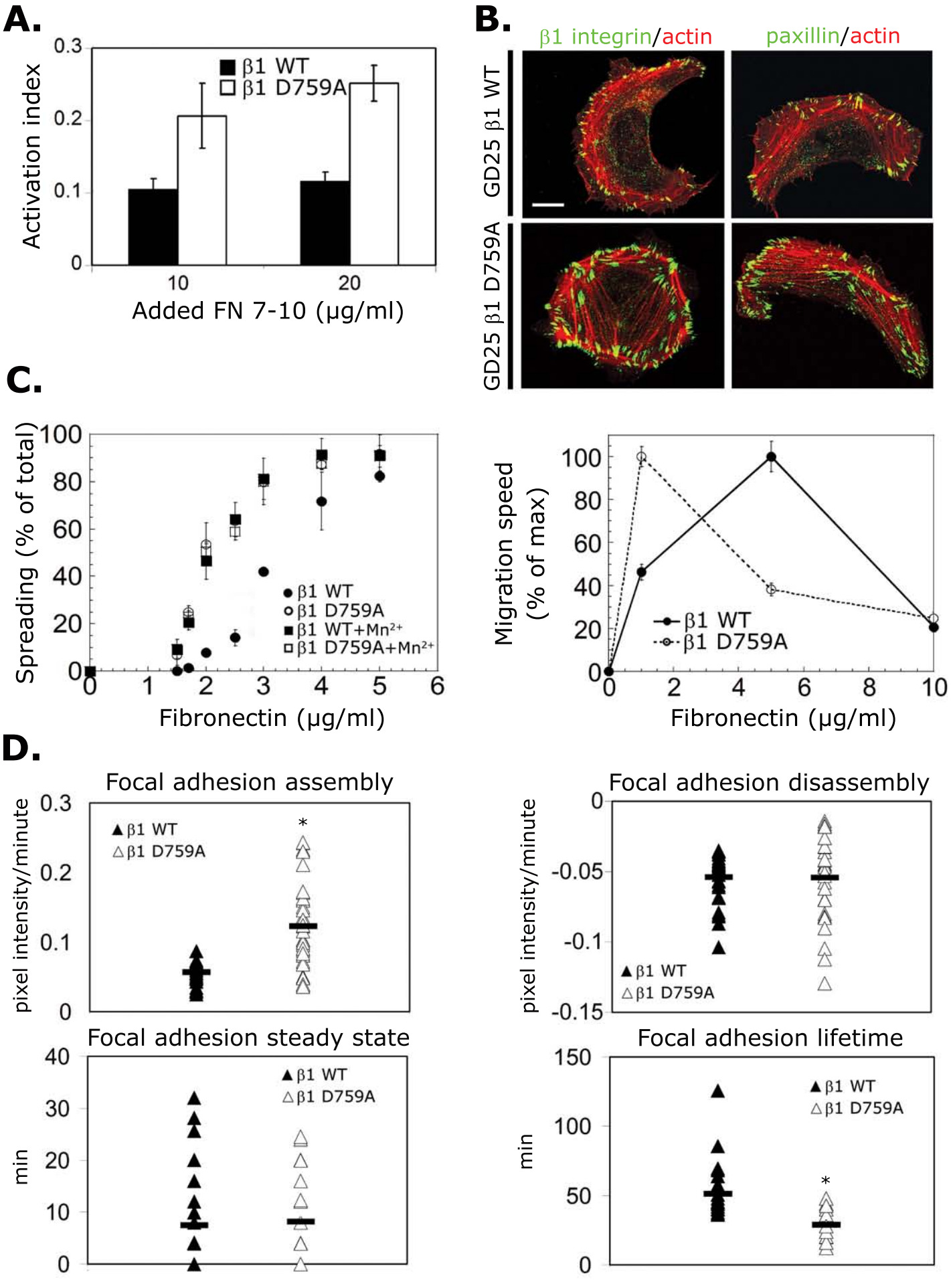

Figure 7. Millon Fremillon A. et al,

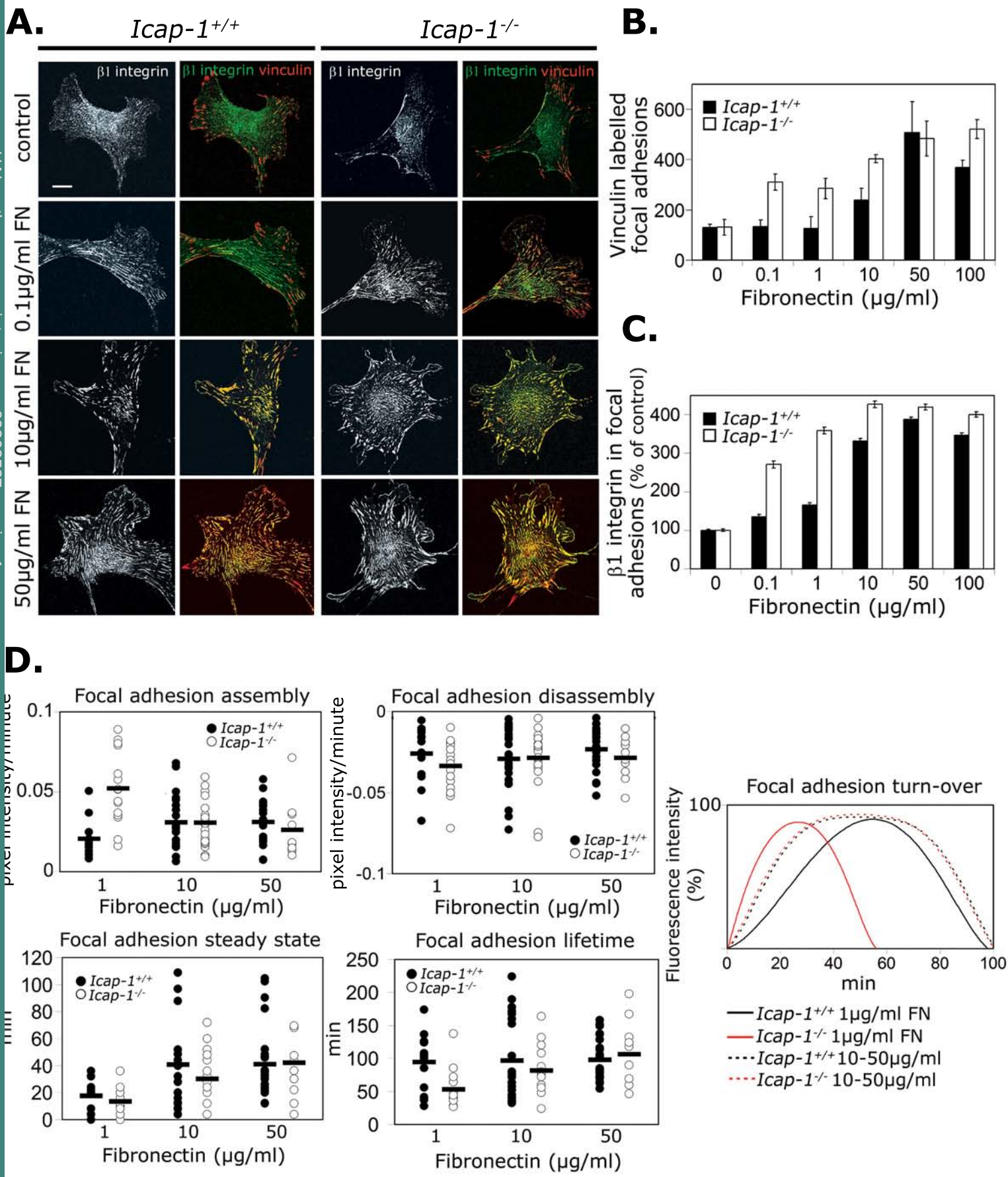

Figure 8. **Millon Fremillon A. et al,**

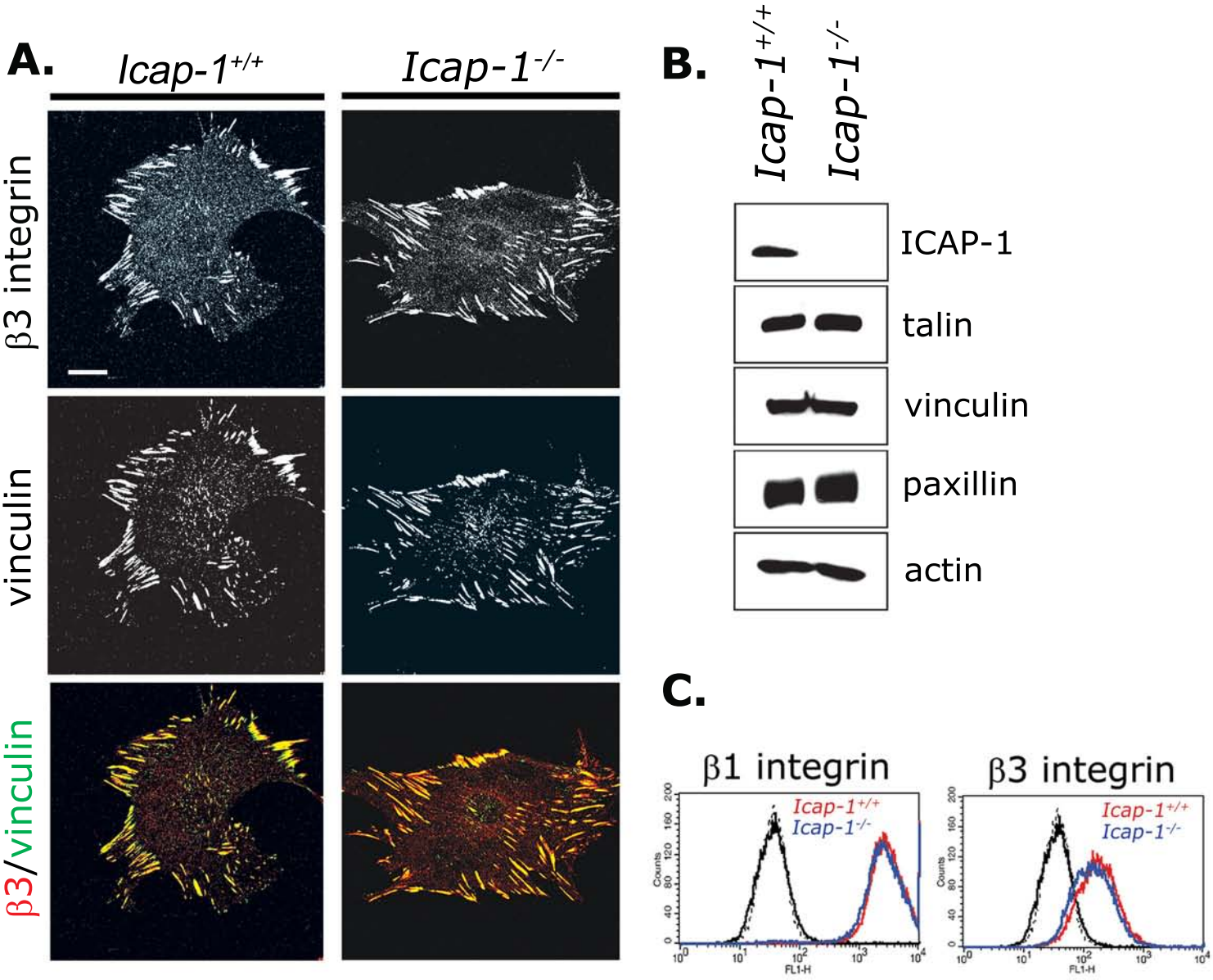

Figure S1. **Millon Fremillon A. et al,**

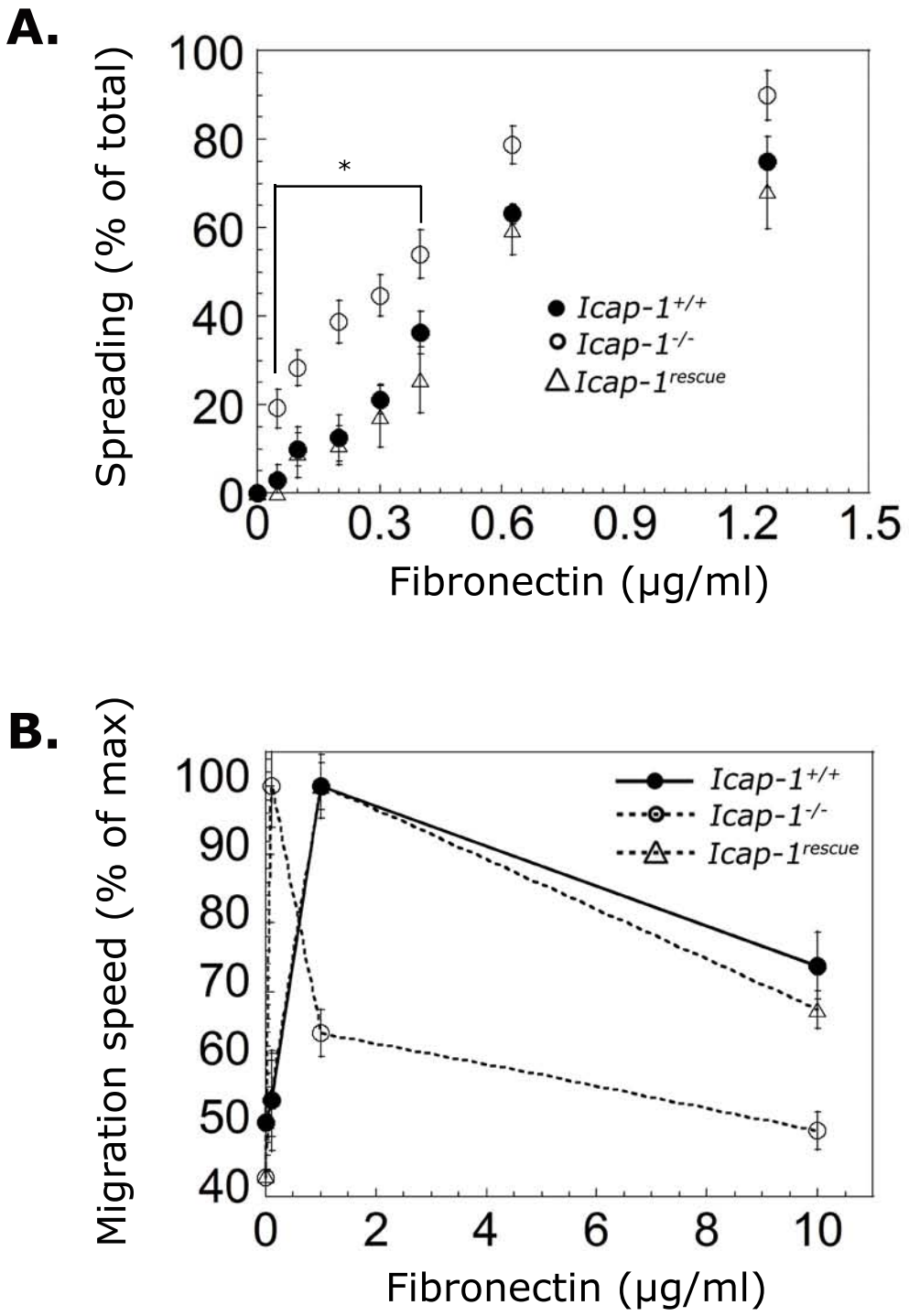

Figure S2. Millon Frémillon A. et al,

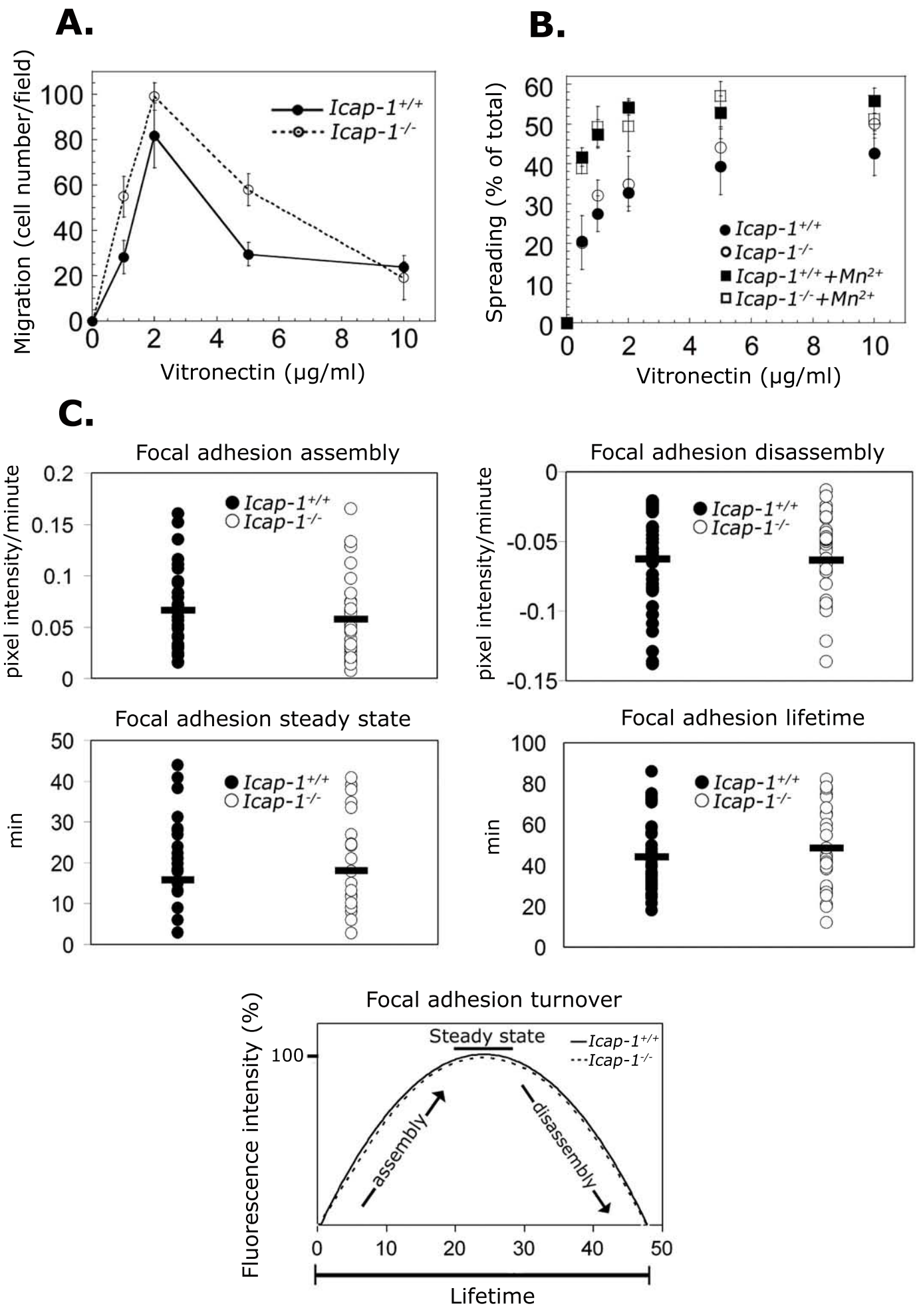

Figure S3. Millon Fremillon A. et al,

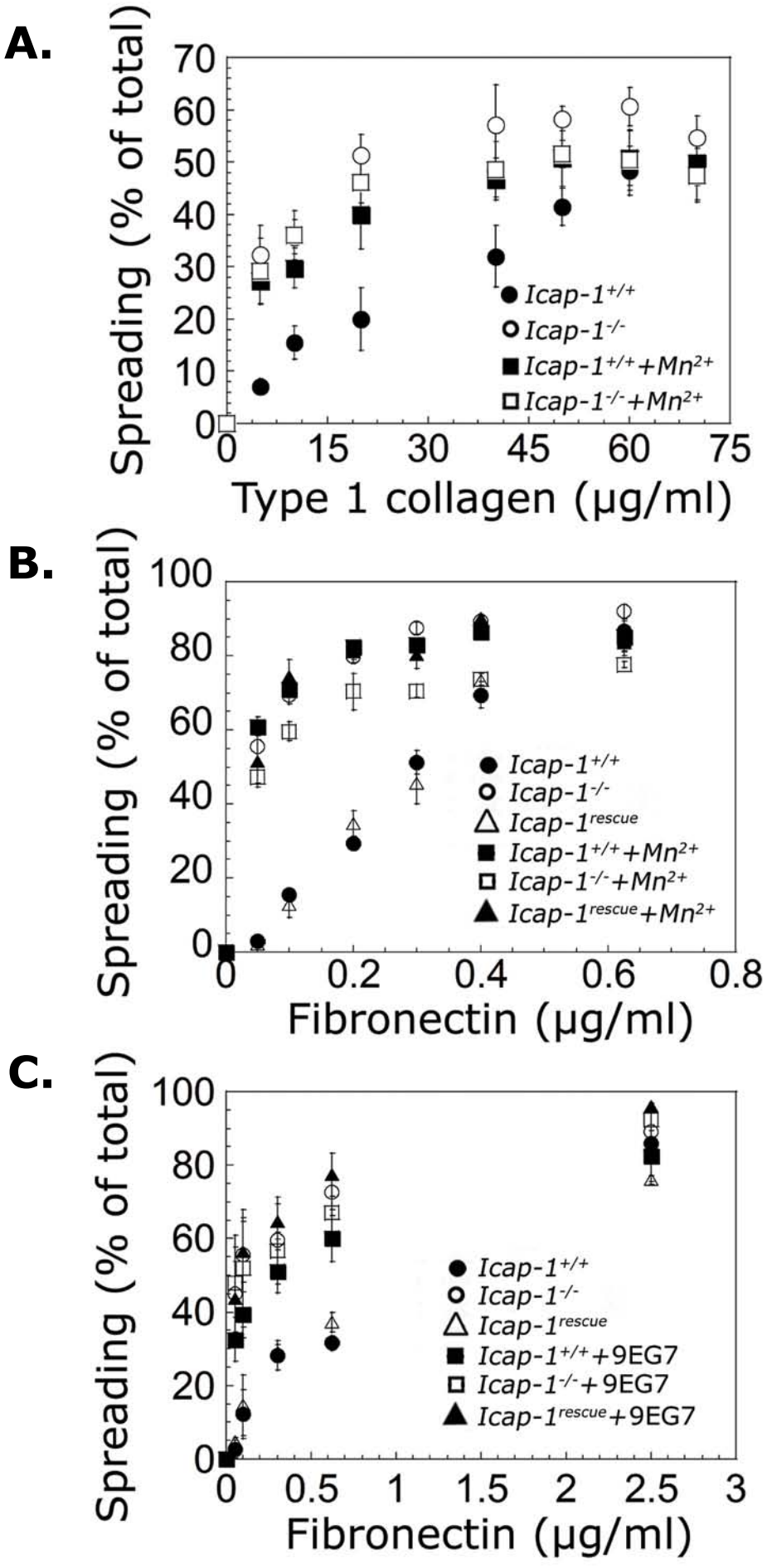

Figure S4. Millon Fremillon A. et al,